ORTA DOĞU TEKNİK ÜNİVERSİTESİ
FEN BİLİMLERİ ENSTİTÜSÜ MÜDÜRLÜĞÜ

TEZ ŞABLONU ONAY FORMU
THESIS TEMPLATE CONFIRMATION FORM

1. Şablonda verilen yerleşim ve boşluklar değiştirilmemelidir.
2. **Jüri tarihi** Başlık Sayfası, İmza Sayfası, Abstract ve Öz'de ilgili yerlere yazılmalıdır.
3. İmza sayfasında jüri üyelerinin unvanları doğru olarak yazılmalıdır. Tüm imzalar **mavi pilot kalemle** atılmalıdır.
4. **Disiplinlerarası** programlarda görevlendirilen öğretim üyeleri için jüri üyeleri kısmında tam zamanlı olarak çalıştıkları anabilim dalı başkanlığının ismi yazılmalıdır. Örneğin: bir öğretim üyesi Biyoteknoloji programında görev yapıyor ve biyoloji bölümünde tam zamanlı çalışıyorsa, İmza sayfasına biyoloji bölümü yazılmalıdır. İstisnai olarak, disiplinler arası program başkanı ve tez danışmanı için disiplinlerarası program adı yazılmalıdır.
5. Tezin **son sayfasının sayfa** numarası Abstract ve Öz'de ilgili yerlere yazılmalıdır.
6. Bütün chapterlar, referanslar, ekler ve CV sağ sayfada başlamalıdır. Bunun için **kesmeler** kullanılmıştır. **Kesmelerin kayması** fazladan boş sayfaların oluşmasına sebep olabilir. Bu gibi durumlarda paragraf (¶) işaretine tıklayarak kesmeleri görünür hale getirin ve yerlerini **kontrol edin**.
7. Figürler ve tablolar kenar boşluklarına taşmamalıdır.
8. Şablonda yorum olarak eklenen uyarılar dikkatle okunmalı ve uygulanmalıdır.
9. Tez yazdırılmadan önce PDF olarak kaydedilmelidir. Şablonda yorum olarak eklenen uyarılar PDF dokümanında yer almamalıdır.
10. **Bu form aracılığıyla oluşturulan PDF dosyası arkalı-önlü baskı alınarak tek bir spiralli cilt haline getirilmelidir.**
11. Spiralli hale getirilen tez taslağınızdaki ilgili alanları imzalandıktan sonra, Tez Juri Atama Formu ile birlikte bölüm sekreterliğine teslim edilmelidir.
12. Tez taslaklarının kontrol işlemleri tamamlandığında, bu durum öğrencilere METU uzantılı öğrenci e-posta adresleri aracılığıyla duyurulacaktır.
13. Tez yazım süreci ile ilgili herhangi bir sıkıntı yaşarsanız, **Sıkça Sorulan Sorular (SSS)** sayfamızı ziyaret ederek yaşadığınız sıkıntıyla ilgili bir çözüm bulabilirsiniz.

1. Do not change the spacing and placement in the template.
2. Write **defense date** to the related places given on Title page, Approval page, Abstract and Öz.
3. Write the titles of the examining committee members correctly on Approval Page. **Blue ink** must be used for all signatures.
4. For faculty members working in **interdisciplinary programs**, the name of the department that they work full-time should be written on the Approval page. For example, if a faculty member staffs in the biotechnology program and works full-time in the biology department, the department of biology should be written on the approval page. Exceptionally, for the interdisciplinary program chair and your thesis supervisor, the interdisciplinary program name should be written.
5. Write **the page number of the last page** in the related places given on Abstract and Öz pages.
6. All chapters, references, appendices and CV must be started on the right page. **Section Breaks** were used for this. **Change in the placement** of section breaks can result in extra blank pages. In such cases, make the section breaks visible by clicking paragraph (¶) mark and **check their position.**
7. All figures and tables must be given inside the page. Nothing must appear in the margins.
8. All the warnings given on the comments section through the thesis template must be read and applied.
9. Save your thesis as pdf and Disable all the comments before taking the printout.
10. **Print two-sided the PDF file that you have created through this form and make a single spiral bound.**
11. Once you have signed the relevant fields in your thesis draft that you spiraled, submit it to the department secretary together with your Thesis Jury Assignment Form.
12. This will be announced to the students via their METU students e-mail addresses when the control of the thesis drafts has been completed.
13. If you have any problems with the thesis writing process, you may visit our **Frequently Asked Questions (FAQ)** page and find a solution to your problem.

☒ **Yukarıda bulunan tüm maddeleri okudum, anladım ve kabul ediyorum. / I have read, understand and accept all of the items above.**

Name : **Mehmet**
Surname : **Tabak**
E-Mail : **e185212@metu.edu.tr**
Date :
Signature : _____

WAVEFRONT SHAPING OPTIMIZATION ALGORITHMS FOR FOCUSING LIGHT THROUGH A MULTIMODE FIBER

A THESIS SUBMITTED TO
THE GRADUATE SCHOOL OF NATURAL AND APPLIED SCIENCES
OF
MIDDLE EAST TECHNICAL UNIVERSITY

BY

MEHMET TABAK

IN PARTIAL FULFILLMENT OF THE REQUIREMENTS
FOR
THE DEGREE OF MASTER OF SCIENCE
IN
PHYSICS

MAY 2022

Approval of the thesis:

WAVEFRONT SHAPING OPTIMIZATION ALGORITHMS FOR FOCUSING LIGHT THROUGH A MULTIMODE FIBER

submitted by **Mehmet Tabak** in partial fulfillment of the requirements for the degree of **Master of Science** i**n Physics, Middle East Technical University** by,

Prof. Dr. Halil Kalıpçılar
Dean, Graduate School of **Natural and Applied Sciences** _____

Prof. Dr. Seçkin Kürkçüoğlu
Head of the Department, **Physics** _____

Assoc. Prof. Dr. Emre Yüce
Supervisor, **Physics, METU** _____

Examining Committee Members:

Prof. Dr. İsa Navruz
Electrical and Electronics Enginnering, Ankara University _____

Assoc. Prof. Dr. Emre Yüce
Physics, METU _____

Assist. Prof. Dr. Ihor Pavlov
Physics, METU _____

Date: 18.05.2022

I hereby declare that all information in this document has been obtained and presented in accordance with academic rules and ethical conduct. I also declare that, as required by these rules and conduct, I have fully cited and referenced all material and results that are not original to this work.

Name Last name : Mehmet Tabak

Signature :

ABSTRACT

WAVEFRONT SHAPING OPTIMIZATION ALGORITHMS FOR FOCUSING LIGHT THROUGH A MULTIMODE FIBER

Tabak, Mehmet
Master of Science, Physics
Supervisor : Assoc. Prof. Dr. Emre Yüce

May 2022, 66 pages

Optical fibers are widely used to guide optical signals. Multi-mode fibers offer a greater bandwidth when compared to single-mode counterparts. The intensity at the end of a multi-mode fiber can be affected by mode-to-mode coupling and multi-mode interference. This can reduce the signal throughput. However, the total intensity at the end of the fiber can be modulated by shaping the input wavefront and providing increased signal levels. In our study, we show that focusing light inside the optical fiber is possible by wavefront shaping. There is a unique wavefront that focuses light inside the media at a given location. While the light moves in the particles, we adjust the wavefront dynamically using the spatial light modulator. Here, we experimentally evaluate and develop optimization algorithms for wavefront shaping that focuses light through a multi-mode fiber. These algoritmhs are continuous sequential (C), stepwise sequential (S), segmented (SE), hybrid Monte-Carlo continuous (MCC), hybrid stepwise continuous (SC) and hybrid segmented continuous (SEC). We analyze and compare these algorithms according to their performance: speed, regional enhancement, total enhancement. The continuous algorithm has reached to focus faster than others, the MCC algorithm is slowest with 46% lower than the C algorithm. The ranking of speed is C, SE, S, SC,

SEC, MCC, in order. However, focus formation is much faster using the H-MCC algorithm. There is focus formation with enhancement 150 times than the initial value at 357 seconds for MCC. The focus is seen clearly at the target point. For regional enhancement, the C algorithms have higher performance than the stepwise with 1.1% and segmented 2.9%. For the total enhancement, the SC algorithm has increased the total transmisson 5.82 times than initial value. The ranking of total enhancement is follow: the C algorithm: 5.80, the S: 5.61, the SE: 5.47, the SEC: 4.97, MCC: 4.90.

Keywords: Interference, Optical fiber, Optimization, Speckle Pattern, Wavefront Shaping

ÖZ

IŞIĞI DALGA ÖNÜ ŞEKİLLENDİRMESİ İLE ÇOK MODLU FİBER İÇİNDE ODAKLANMASINI SAĞLAYAN OPTİMİZASYON ALGORİTMALARI

Tabak, Mehmet
Yüksek Lisans, Fizik
Tez Yöneticisi: Doç. Dr. Emre Yüce

Mayıs 2022, 66 sayfa

Optik fiberler, optik sinyalleri yönlendirmek için yaygın olarak kullanılmaktadır. Çok modlu fiberler, tek modlu muadillerine kıyasla daha büyük bir bant genişliği sunar. Çok modlu bir fiberin sonundaki yoğunluk, moddan moda bağlama ve çok modlu girişimden etkilenebilir. Bu, sinyal verimini azaltabilir. Bununla birlikte, fiberin sonundaki toplam yoğunluk, giriş dalga cephesini şekillendirerek ve artan sinyal seviyeleri sağlayarak modüle edilebilir. Çalışmamızda, fiber optik içerisinde ışığı odaklamanın dalga cephesi şekillendirme ile mümkün olduğunu gösterdik. Medyanın içindeki ışığı belirli bir konuma odaklayan benzersiz bir dalga cephesi vardır. Işık ortam içinde hareket ederken ışığın dalgasını dinamik olarak uzaysal ışık modülatörü ile ayarlanmaktadır. Bu tezde, ışığı saçan bir nesne aracılığıyla odaklayan dalga cephesi şekillendirme için optimizasyon algoritmalarını deneysel olarak değerlendiriyor ve geliştiriyoruz. Bu algoritmalar, sürekli sıralı (C), kademeli sıralı (S), segmentli (SE), Monte-Carlo sürekli hibrit (MCC), kademeli sürekli hibrit (SC) ve segmentli sürekli hibrit (SEC) olarak isimlendirilmektedir. Bu algoritmaları hızlarına, fiberin içinde seçilen bölgesel ışık artış miktarı ve fiberdeki total ışık miktarındaki artışa göre performanslarını analiz ediyor ve karşılaştırıyoruz. Sürekli

algoritma seçilen noktada odaklanmayı en hızlı gerçekleştirilen algoritma oldu, en yavaş algoritma olarak hibrit Monte-Carlo sürekli olmuştur ve sürekli algoritmaya göre yaklaşık %46 daha yavaş ışığı istenilen noktaya odaklamıştır. Hızların algoritmalara arası sıralaması şu şekilde ölçülmüştür: Sürekli sıralı, segmenti, kademeli sıralı, hibrit kademeli sürekli, hibrit segmentli sürekli ve hibrit Monte-Carlo sürekli. Hibrit Monte-Carlo sürekli algoritmasında diğerlerinden çok daha önce odak oluşumu gözlemlenmiştir. Algoritma başladıktan sonra 357. saniyede seçilen hedef noktasında ışık artış miktarı ilk ışık miktarının yaklaşık 150 katına çıkmıştır. Aynı süre zarfında diğer hiçbir algoritmada herhangi bir değişiklik gözlenlenmemiştir. Bölgesel bölgedeki artış miktarında, sürekli sıralı algoritması kademeli sıralı algoritmaya göre %1,1 ve segmentli algoritmaya göre %2.9 daha iyi performans göstermiştir. Toplam ışık miktarındaki artış miktarında ise hibrit kademeli sürekli algoritma başlangıç değerinin yaklaşık 5.82 katına artırmıştır. Diğer algoritmaların performansı: sürekli sıralı 5.80, kademeli sıralı 5.61, segmentli 5.47, hibrit segmentli sürekli 4.97, hibrit Monte-Carlo sürekli 4.90 olarak gözlemlenmiştir.

Anahtar Kelimeler: Dalga Önü Şekillendirilmesi, Optical Fiber, Girişim, Optimizasyon, Alacalı Desen

Dedication to My Mother, My Father and My Wife

ACKNOWLEDGMENTS

This study is supported by The Scientific and Technological Research Council of Turkey (TÜBİTAK), grant no 118M199, 116C074 and TÜBA-GEBİP. We would like to thank Alpan Bek and Allard P. Mosk for providing us the essential equipment.

I would like to express my gratitude to my supervisor, Assoc. Prof. Dr. Emre Yüce for her continuous and invaluable guidance, advice, encouragements, patience and criticism throughout the research. Without his trust and guidance, I can hardly finish my work.

I apriciate my lab mates; Deniz Bender, Berk Nezir Gün and Gılda Afshari and Süleyman Kahraman.

I am thankful to my manager Dilek Candan for supporting and encouraging my master's. Also, I would like to thank my colleagues Tuğçe Başer, Seda Şirin, Serkan Üçer, Salih Hacialioğlu, and Batıhan Konuk.

I would also like to thank specially to Merve Kilic and Kübra Cerit for their friendship and support since I started university and especially during my master's years.

I would like to thank my mom and dad; Ümmühan Tabak, Şaban Tabak for their endless love and encouragement, and I want to thank my sisters Yasemin Tabak, Nurcan Tabak and Elif Tabak for understanding and supporting during my master study. Also, I would like to thanks my father-in-law and mother-in-law; Özcan Dumanlılar and Halide Dumanlılar for supporting and encouraging to finish my thesis.

Finally and foremost, I would like to special thank to my wife Beril Dumanlılar for her love, support and understanding during my entire METU life. Also, I appriciate my cat Fiko Bey for sharing many moments with us.

TABLE OF CONTENTS

ABSTRACT v

ÖZ vii

ACKNOWLEDGMENTS x

TABLE OF CONTENTS xii

LIST OF TABLES xiv

LIST OF FIGURES xv

LIST OF ABBREVIATIONS xx

CHAPTERS

1 INTRODUCTION 1

1.1 Light Propagation in Multimode Media 1

1.2 Spatial Light Modulator 3

1.3 Focusing Light Through Multimode Fiber 4

1.4 In This Thesis 5

2 THEORY 7

2.1 Waveguide Structure 7

2.2 Light Behaviour in Scattering Materials 9

2.2.1 Propagation of Light in Homogenous Media 9

2.2.2 Propagation of Light in Inhomogeneous Media 10

2.2.3 Light Propagation in Optical Fiber 11

2.3 Mixing Channel 13

2.3.1 Scattering Channels 13
2.3.2 Intensity Distribution of Speckle Pattern 13
2.4 Wavefront Shaping Process 15
2.4.1 Physics Behind of Wavefront Shaping Process 15
2.4.2 Maximum Intensity Enhancement 16
3 EXPERIMANTAL SETUP 19
3.1 Setup 19
3.2 Experiment 20
3.2.1 Optimization Algorithms for Focusing Light through Turbid Media 23
4 RESULTS AND DISCUSSION 29
4.1 Phase Control Algorithms for Focusing Light 29
4.1.1 Speed of Six Phase Control Algorithms 29
4.1.2 Enhancement of Six Phase Control Algorithms 35
5 CONCLUSION 59
REFERENCES 61

LIST OF TABLES

TABLES

Table 1 Show the three algorithms single iteration times,complete repetition times and total operation times 32
Table 2 Show the total elapsed time and iteration number until the visible focus formation 33
Table 3 Show the performance of six algorithms at the beginning 34
Table 4 Show the screenshot of each algorithm at 357 seconds 34
Table 5 Show the summary of the regional enhancement of six algorithms..... 54
Table 6 Summary of the total enhancement of six algorithms 56

LIST OF FIGURES

FIGURES

Figure 1.1 A plane wave hits on an opaque scattering media. In the media, light performs random propagate. The random walk leads to scattering light in all directions [6]. 1
Figure 1.2 transmitted intensity of the scattered light in the fiber optic cable. Random interference pattern, known as a laser speckle, is formed from the scattered light. Inset, at each point many waves interfere randomly, this results in a low overall intensity. 2
Figure 1.3 Interference in a multimode fiber. (**a)** Before unshaped the incident beam, light interfere randomly due to scattering. (**b)** The incident light is shaped and tranmitted intensity is focused at the target point. The intensity is almost 1000 times higher than the average intensity of the speckle pattern shown **a** [6]. 4
Figure 1.4 (**a)** A incident beam crashes on tiny particles in the medium. The light propagates in all direction lose their directionality due to scattering. (**b)** The incident light is shaped considering the scattering media and the light is focused to any target point by the shaped wave. 5
Figure 2.1 Basic appearance of fiber optic cable [36]. 7
Figure 2.2 Transmission of light in the fiber. Light is propagated with in the fiber since the total internal reflaction occurs between the core and claddeing interferance [36]. 8
Figure 2.3 Basic speckle pattern. This is representation of the energy pattern that is appears at the end of a fiber. 14
Figure 2.4 Description of channels demixing with complex amplitude representation of the field. In (a) the initial case is explained. All channels contribution is randomly at the total field. In (b) all phase are cycled to find the field transmission coefficient. The red lines and dashes line represent the adjusted phase. In (c) all phase is set to right shift since all transmission coefficient are known, all phase are in phase at the target positon. 15

Figure 3.1 The laser emits lights (1), camera monitors the light at the end of fiber cable (2), beam expander increase the beam size (3), the SLM modulate the phase of light (4), lenses compress the light before the fiber (5), and light is coupled to the fiber cable (6).....19
Figure 3.2 Feedback method for achieving optimization algorithms for wavefront shaping. An incident beam is shaped by SLM (1) and these shaped beam enter into optical fiber (2), a detector (3) detect the total transmitted light that reaches the target area. A feedback algorithm (4) uses the signal from the detector to program the phase modulator. Before the algorithm is started, the transmitted light forms a random speckle pattern. The algorithm changes the incident wave to increase the intensity in the target area. After a few iterations, the transmitted light focuses on the target. 20
Figure 3.3 A schematic representation of the super-pixel. A single super- pixel corresponce to the 30×30 pixels. 21
Figure 3.4 Represantation of five gray scale values that are used in algorithms. ...22
Figure 3.5 Monte Carlo algorithm, variables in Eq. 3.2 except x and y are created randomly for each iteration and the SLM is updated after each iteration. 23
Figure 3.6 Monte Carlo Algorithm Diagram.....24
Figure 3.7 the continuous sequential algorithm, all segment are addressed sequentially, after the optimal phase is determined for each superpixels, the SLM is updated after each iteration (red squares). 25
Figure 3.8 the stepwise sequential algorithm, after the optimal phase is determined for all superpixels, the SLM is updated to construct the optimal wavefront. 26
Figure 3.9 the segmented algorithm, randomly selects of one of superpixels and adjusts their optimal phase, the SLM is updated after each iteration. 26
Figure 4.1 Time versus enhancement of the continuous, stepwise and segmented algorithms, the green, red and black rods are the complete repetition point of continuous.....31
Figure 4.2 Time versus enhancement of six algoritmhs.....32

Figure 4.3 Tranmission intensity distribution through a fiber optic cable, (a) Transmission before optimisation with unshaped wavefront, all pixels have low intensity, (b) Transmission after optimisation with shaped wavefront, the selected point is highlighted in a red square. The transmission after optimisation in the selected point is 318 times brighter than the before optimisation..... 37
Figure 4.4 The target 5×5 pixels area in the fiber cable. After optimisation, scattered light is focussed at the target with shaped wavefront. 38
Figure 4.5 The cross section of the target point. (a) all pixels intensity before optimisation, (b) all pixels intensity after optimisation, target point pixels did not exceed the 256..... 39
Figure 4.6 Tranmission intensity distribution through a fiber optic cable, (a) Transmission before optimisation with unshaped wavefront, all pixels have low intensity, (b) Transmission after optimisation with shaped wavefront, the selected point is highlighted in a red square. The transmission after optimisation in the selected point is 301 times brighter than the before optimisation..... 40
Figure 4.7 The target 5×5 pixels area in the fiber cable. After optimisation, scattered light is focussed at the target with shaped wavefront. 41
Figure 4.8 The cross section of the target point. (a) all pixels intensity before optimisation, (b) all pixels intensity after optimisation, target point pixels did not exceed the 256..... 42
Figure 4.9 Tranmission intensity distribution through a fiber optic cable, (a) Transmission before optimisation with unshaped wavefront, all pixels have low intensity, (b) Transmission after optimisation with shaped wavefront, the selected point is highlighted in a red square. The transmission after optimisation in the selected point is 298 times brighter than the before optimisation..... 43
Figure 4.10 The target 5×5 pixels area in the fiber cable. After optimisation, the light is focussed at the target with shaped wavefront. 44
Figure 4.11 The cross section of the target point. (a) all pixels intensity before optimisation, (b) all pixels intensity after optimisation, target point pixels did not exceed the 256..... 45

Figure 4.12 Tranmission intensity distribution through a fiber optic cable, (a) Transmission before optimisation with unshaped wavefront, all pixels have low intensity, (b) Transmission after optimisation with shaped wavefront, the selected point is highlighted in a red square. The transmission after optimisation in the selected point is 293 times brighter than the before optimisation. 46
Figure 4.13 The target 5×5 pixels area in the fiber cable. After optimisation, scattered light is focussed at the target with shaped wavefront. 47
Figure 4.14 The cross section of the target point. (a) all pixels intensity before optimisation, (b) all pixels intensity after optimisation, target point pixels did not exceed the 256. 48
Figure 4.15 Tranmission intensity distribution through a fiber optic cable, (a) Transmission before optimisation with unshaped wavefront, all pixels have low intensity, (b) Transmission after optimisation with shaped wavefront, the selected point is highlighted in a red square. The transmission after optimisation in the selected point is 318 times brighter than the before optimisation. 49
Figure 4.16 The target 5×5 pixels area in the fiber cable. After optimisation, scattered light is focussed at the target with shaped wavefront. 50
Figure 4.17 The cross section of the target point. (a) all pixels intensity before optimisation, (b) all pixels intensity after optimisation, target point pixels did not exceed the 1. 51
Figure 4.18 Tranmission intensity distribution through a fiber optic cable, (a) Transmission before optimisation with unshaped wavefront, all pixels have low intensity, (b) Transmission after optimisation with shaped wavefront, the selected point is highlighted in a red square. The transmission after optimisation in the selected point is 318 times brighter than the before optimisation. 52
Figure 4.19 The target 5×5 pixels area in the fiber cable. After optimisation, scattered light is focussed at the target with shaped wavefront. 53
Figure 4.20 The cross section of the target point. (a) all pixels intensity before optimisation, (b) all pixels intensity after optimisation, target point pixels did not exceed the 256. 54

Figure 4.21 Regional enhancement of six algorithms, the performance rank is SC, SEC, C, S, SE, MCC respectively. 55
Figure 4.22 Representing total enhancement versus iteration number of six algorithms 58

LIST OF ABBREVIATIONS

ABBREVIATIONS	
MC-C	Monte Carlo Continuous
NA	Numerical Aperture
SC	Stepwise Continuous
SEC	Segmented Continuous
SLM	Spatial Light Modulator
2D	Two Dimensional

CHAPTER 1

INTRODUCTION

1.1 Light Propagation in Multimode Media

Devices using or producing light have become an essential part of modern life. In daily life, light is using numerous application such as display, communication, and sensing applcations. Optical techniques are crucial and indispensable to enhance technology in the industry, medicine, agriculture, and scientific research [1, 2].

Light travels along a straight line in a homogenous medium such as air. However, light lose their directionality in non-homogenous materials, like paper or human tissue, due to the multiply scattering of light [3, 5]. Such non-homogeneous materials contain a microscopic structure that makes it impossible to propagate along a straight line [6, 7]. Figure 1.1 expresses what occurs when a beam of light hits on a white object: collisions with the microscopic structure result in the light diffusing and losing out their directionality [8].

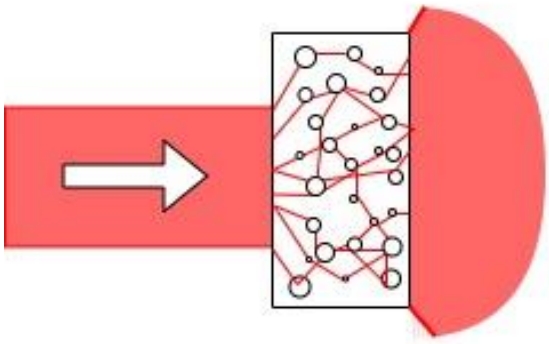

Figure 1.1 A plane wave hits on an opaque scattering media. In the media, light performs random propagate. The random walk leads to scattering light in all directions [6].

Scattering and diffusion of light put huge constrain on optical imaging, communication, spectroscopy, and other optical applications [9, 10]. There was a great effort to develop imaging methods that work in strongly scattering media in the past twenty years [11, 12].

Huygens's principle explains more understandable how the wave propagates in the scattering media [13]. Part of the light is diffuse when the incident beam crash the tiny microscopic particles. This crash forms a spherical wave that moves away from the particle [14]. The spherical wave crashes other tiny particles, its leads to more and more waves [15]. Therefore, light propagation is highly complex in the scattering media. Incident light is scattered thousands times until arriving on the other side of the sample.

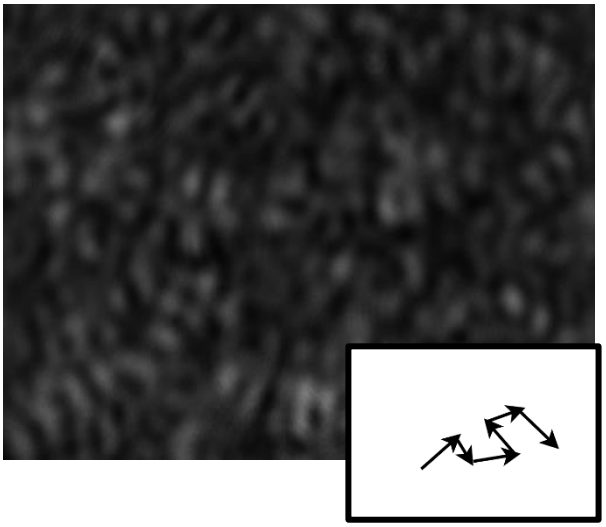

Figure 1.2 Transmitted intensity of the scattered light in the fiber optic cable. Random interference pattern, known as a laser speckle, is formed from the scattered light. Inset, at each point many waves interfere randomly, this results in a low overall intensity.

The fiber cable is used for enhancing transmitted intensity [16-18]. Interference many different waves that after hitting a particle in the sample form the complicated random pattern Figure 1.2.

Optical fibers are capable of guiding a light beam over long distances or along disordered media like biological tissues. While the information traveling along the fiber, the intensity at the end of the fiber can be easily control from the input side. However, multimodes fibers can emit a light beam that has much information using its expansion in the propagating modes. As a result, a random speckle pattern is always obtained at the output of a multimode fiber. Therefore, multimode fiber can be thought of as a strongly scattering media.

1.2 Spatial Light Modulator

A spatial light modulator (SLM) is a device that can adjust the light by modulating the amplitude and phase of incident light [19, 20]. SLM device converts the data from electromagnetic signals to electronic format. SLM is a programmable device to modulate light output based on a particular pixel combination [21]. Fundamentally transmitted light that is controlled in phase only, amplitude only, or both [22]. In our case, the phase-only modulation setup is used. The SLM includes liquid crystals that react to applied voltage via its birefringent feature. Different applied voltages on the SLM result in varying phase shifts depending on refractive indices [23]. The relation between voltage and phase shift could be linear or nonlinear, and the relation can be adjustable for a specific wavelength.

Thanks to the control algorithm, a phase-only SLM loads the images over the surface of itself with ~60 Hz refresh rate. This is crucial experimental advantages. In our work, it is considered the linear changes in the phase shift like a function of grey scales as if using monochromatic light. The detail information will be explain in chapter 4. Some of works in this field are laser processing [24], optical imaging [25], computer-generated holograms [26], and signal processing [27]. In the field of biomedical research application, Vellekoop and Mosk are put remarkable method to focus light inside disordered media [28].

1.3 Focusing Light Through Multimode Fiber

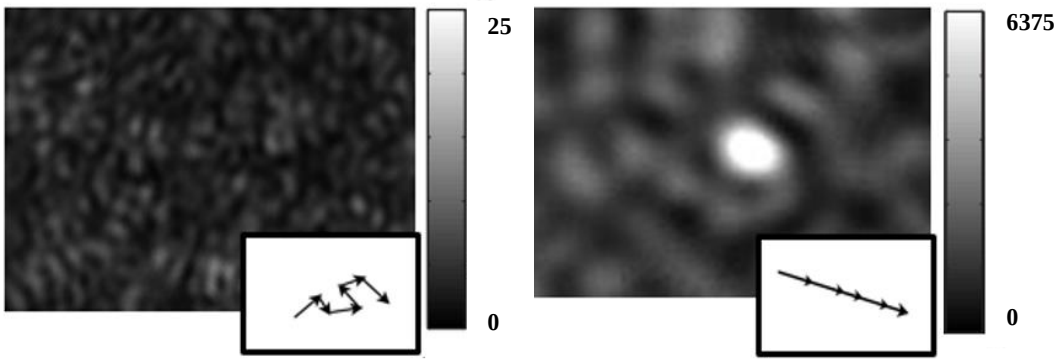

(a) (b)

Figure 1.3 Interference in a multimode fiber. (**a)** Before unshaped the incident beam, light interfere randomly due to scattering. (**b)** The incident light is shaped and tranmitted intensity is focused at the target point. The intensity is almost 1000 times higher than the average intensity of the speckle pattern shown **a** [6].

The wavefront shaping technique is widely used to focus light inside the disordered media [29, 30]. There is a special incident wavefront that makes focus light at the target position. In our study, we use the inverse diffusion wavefront method to focus light inside the media Figure 1.3. Our experiment study is as follows. The fiber optic cable is considered a disordered media [31, 32]. Once we illuminate the fiber with coherent light, a speckle pattern occurs. The constructive and destructive interference of light inside the media is caused to this pattern. While the light travels throughout the media, change its phases due to scattered multiple times. Under coherent light illumination, the wave interference will be random and unconnected to each other. There is no position inside the media where all wave contributions are in phase. If we want to focus light on the target position, all wave contributions should interfere constructively at the target point. We control and adjust the independent wave contributions using a spatial light modulator (SLM). With this SLM we can control each phase of the wave to find the optimal relative phases of each contribution by

modulating one by one.The superpixel technıque is used to perfom the experimand and one superpixel has been grouped into 30x30 micro pixels onto SLM [33, 34]. Therefore, we deduce that the incident wavefront turns into an optimum wavefront that all relative phases interfere constructively at the target position.

1.4 In This Thesis

The purpose of this thesis is to construct optimization algorithms that optimally focus the light at the target point via wavefront shaping Figure 1.4. The optimisation algorithms is developed for full spatial phase control of a laser beam using SLM.

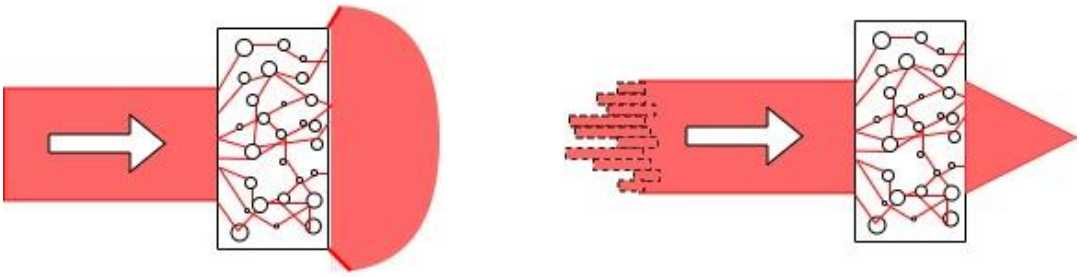

(a) (b)

Figure 1.4 (**a)** A incident beam crashes on tiny particles in the medium. The light propagates in all direction lose their directionality due to scattering. (**b)** The incident light is shaped considering the scattering media and the light is focused to any target point by the shaped wave.

Here, we present six different algorithms that find the optimal incident wavefront when the scattering media is perfectly fixed and the noise level is negligible. These algorithms are compared according to their dynamic behaviour and performance such as speed, total enhancement, and regional enhancement. A computer program is used to create and perform all algorithms.

Chapter 2 describes the theory of light behaviour and waveguide structure. Propagation of light in the homogeneous, non-homogeneous medium and fiber optic are discussed. Mixing and de-mixing methods are briefly explained.

Chapter 3 gives the setup information in detail. How the experiments are performed and which components are used in this part are explained.

Chapter 4 start with explanation of the method of the experiment. Then, all development algorithms that's are continuous sequential, stepwise sequential, segmented, Monte Carlo are clearly explained.

Chapter 5 present experimental results of the six algorithms. For all of them, intensity increasing at the target area are shown. Performance of total enhancement, regional enhancement and speed are discussed.

Chapter 6 gives the summary of the performed work and possible future work.

CHAPTER 2

THEORY

2.1 Waveguide Structure

The optical fibers consist of two basic parts core and cladding [35]. The Core is the longitudinally extended high-index optical medium, cladding surrounds the core with low-index media as shown in the Figure 2.1.

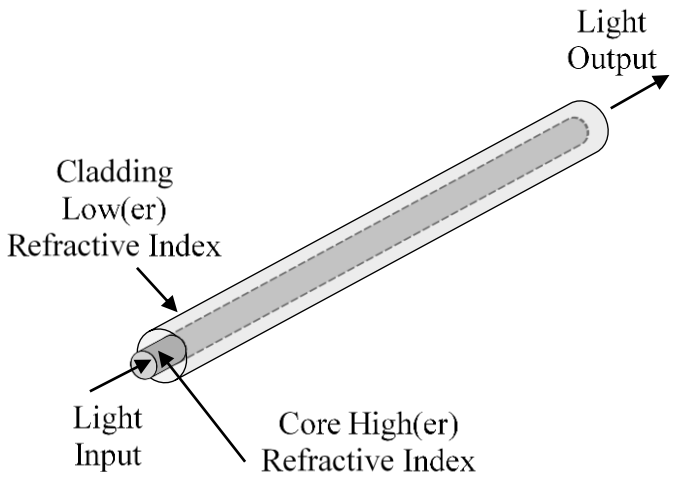

Figure 2.1 Basic appearance of fiber optic cable [36].

The core refractive index n_1 is higher than the cladding index n_0. Hence, total internal reflection confines the light beam coupled to the waveguide's end face in the core [36]. The condition of the total internal reflection between core and cladding interface is given by

$$n_1 \sin(\pi/2 - \emptyset) \geq n_0 \tag{2.1}$$

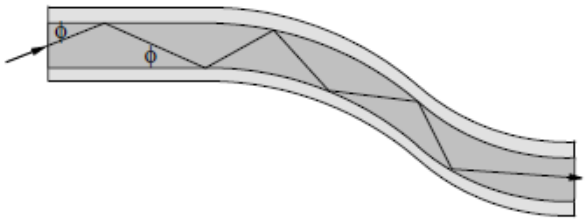

Figure 2.2 Transmission of light in the fiber. Light is propagated with in the fiber since the total internal reflaction occurs between the core and claddeing interferance [36].

The relation between the angle $\emptyset$ and incident beam angle θ are given by $sin\theta = n_1 sin\emptyset \leq \sqrt{n_1^2 - n_0^2}$. Using this equation, we obtain the crucial condition for total internal reflection Figure 2.2 as,

$$\theta \leq sin^{-1}\sqrt{n_1^2 - n_0^2} = \theta_{max} \tag{2.2}$$

The difference in refractive indices between the core and the cladding is on the order of $n_1 - n_0 = 0.01$. Using Eq. (2.1), the θ_{max} can be calculated as

$$\theta_{max} \cong \sqrt{n_1^2 - n_0^2}\,. \tag{2.3}$$

θ_{max} indicates the maximum light acceptance angle of the waveguide and it's known as the numerical aperture (NA) [37].

$\emptyset_{max} \cong \theta_{max}/n_1 \cong \sqrt{2\Delta}$ is the maximum angle for propagating light within the core where Δ is the relative refractive index difference between n_1 and n_0 calculated from

$$\Delta = \frac{n_1^2 - n_0^2}{2n_1^2} \cong \frac{n_1 - n_0}{n_1} \tag{2.4}$$

We obtain the relation between the numerical aperture NA and the relative refractive-index difference Δ by

$$NA = \theta_{max} \cong n_1\sqrt{2\Delta} \tag{2.5}$$

2.2 Light Behaviour in Scattering Materials

In this part, the behavior of light inside scattering media is explained. Light propagating through disordered media results in scattering multiple times and diffuses through the media [38]. The diffusion of light is studied theoretically based on Green's functions and multiple scattering theory [39].

In a scattering medium, the light loses their directionality and spread out through the medium [40]. Before the light enters the medium, it can be controlled by sending a specially shaped wavefront that makes the light interference constructive at a desired point [41-44]. Moreover, we can focus the light on any desired position.

To understand the behavior of light inside the scattering media, the propagation of the electric field inhomogeneous medium will be the first discussed. The related Green's function will be derived. The Green's function describing the field propagation in an in homogenous media will derive from the Green's function for a homogenous media. Using the field propagator, we will express the intensity propagator that eventually result with the diffusion equation.

2.2.1 Propagation of Light in Homogenous Media

The Maxwell equations clearly describe the propagation of light [45]. The magnetic and electric field are vector quantities, but describing the vector of light in the scattering media is extremely difficult. If the light is considered as a scalar quantity, we can model the propagation of light. Using the Maxwell equations, the scalar wave equation [46]:

$$\nabla^2\psi(r,t) - \frac{n^2}{c^2}\frac{d^2}{dt}\psi(r,t) = 0 \tag{2.6}$$

Where ψ the complex amplitude of the electric field, n is the refractive index of the medium, c is the speed of light. In a homogenous media, the refractive index is

independent from the position [47]. Taking Fourier transform of Eq. 2.6 with respect to time give us the scalar Helmholtz wave equation

$$-\nabla^2\psi(\mathrm{r},\mathrm{w}) - k^2\psi(r,w) = 0 \tag{2.7}$$

With $k \equiv \frac{nw}{c}$ where w is the angular frequency of the light.

To solve Eq. 2.7 we use the Green' function. The Green's function gives the solution of wave equation that is in presence of a point source at position r^{ι}. The bare Green's function is found in the homogeneous medium by solving,

$$-\nabla^2 g(r,r^{\iota},w) - k^2 g(r,r^{\iota},w) = \delta(r-r^{\iota}) \tag{2.8}$$

Where $\delta(r-r^{\iota})$ is the Dirac δ-function. Then, we found the bare Green's function,

$$g(\tilde{r},w) = -\frac{e^{ik(w)\tilde{r}}}{4\pi\tilde{r}} \tag{2.9}$$

The difference between r and r^{ι} is single parameter for bare Green's function that allows us to write g as a function of $\tilde{r} = r - r^{\iota}$.

2.2.2 Propagation of Light in Inhomogeneous Media

The refractive index is $n(r) \equiv \sqrt{n_0^2 + \Delta n^2(r)}$ for an inhomogeneous media. The refractive index obviously is a function of the position. Here, n_0 the constant refractive index of the background. The time independent wave equation in inhomogeneous media is written:

$$-\nabla^2\psi(r,w) - k^2(w)\psi(r,w) = V(r,w)\psi(r,w) \tag{2.10}$$

Where $V(r,w) \equiv \Delta n^2(r)\frac{w^2}{c^2}$ the position related with the scattering potential. Then, we can rewrite the Green's function that explains the propagation between r^{ι} and r in the inhomogeneous media. Then, the Green's function become:

$$G(r,r^{\iota},w) = g(r-r^{\iota},w) + \int dr_1\, g\big(r-r_{1,w}\big)V(r_1,w)G(r_1,r^{\iota},w) \tag{2.11}$$

2.2.3 Light Propagation in Optical Fiber

2.2.3.1 Boundary Conditions for fiber

The intensity flux is used for calculating the boundary conditions for the material surfaces. The flux, $J(s,r)$, define as rate of energy propagating in a particular direction. The current can found by integrating the flux for all directions,

$$\mathbf{T}(r) = \int_0^{2\pi} \int_0^{\pi} d\theta d\emptyset \sin(\theta) J(s,r)s, \tag{2.12}$$

Where $s = (cos\emptyset sin\theta, sin\emptyset, cos\theta)$. The total intensity is calculated by divided the flux to the average energy velocity v_e.

$$I(r) = \frac{1}{v_e} \int_0^{2\pi} \int_0^{\pi} d\theta d\emptyset \sin(\theta) J(s,r) \tag{2.13}$$

Taking time derivative gives the net flux across infinitely small closed surface,

$$\nabla \mathbf{T} = -\frac{\partial I}{\partial t} \tag{2.14}$$

If we combine the Eq. 2.14 with the diffusion equation,

$$\frac{\partial R(\tilde{r},t)}{\partial t} = D\nabla^2 R(\tilde{r},t) + source \tag{2.15}$$

$$\mathbf{T} = -D\nabla I \tag{2.16}$$

We assume that the incoming and outgoing flux is distributed uniformly over all angles. Then, the outgoing and incoming flux found,

$$\mathbf{T}_{out}(\mathrm{s},\mathrm{r}) = J_{out}/2\pi \tag{2.17}$$

and

$$\mathbf{T}_{in}(s,r) = RJ_{out}/2\pi \tag{2.18}$$

Where the R is the reflection coefficient that is found by integrating the Fresnel reflection coefficients over all angles.

Now, we can calculate the total intensity using the defined flux. (z = 0 and z = L for the left and right boundary respectively).

$$I(r) = \frac{1}{v_e} J_{out}(1 + R) \tag{2.19}$$

$$\nabla I = \frac{1}{D}\int_0^{2\pi} d\emptyset\, J_{out}\left[\int_0^{2\pi} d\theta \sin(\theta)\, s + \int_{\frac{\pi}{2}}^{\pi} d\theta \sin(\theta)\, Rs\right] \tag{2.20}$$

$$= \frac{1}{2D} J_{out}[1 - R]e_z \tag{2.21}$$

For the left boundary condition is found combining these two equations,

$$I(r)|_{z=0} - z_{e_1} \frac{\partial I(r)}{\partial z}|_{z=0} = 0 \tag{2.22}$$

Where z_{e_1} is the extrapolation length at the left boundary (ref) calculated as a

$$z_{e_1} \equiv l_{tr} \frac{2}{3} \frac{1+R}{1-R} \tag{2.23}$$

Similarly, the right boundary conditions is found,

$$I(r)|_{z=L} - z_{e_2} \frac{\partial I(r)}{\partial z}|_{z=L} = 0 \tag{2.24}$$

Where z_{e_2} is the extrapolation length at the left boundary (ref) calculated as a

$$z_{e_2} \equiv l_{tr} \frac{2}{3} \frac{1+R}{1-R} \tag{2.25}$$

2.2.3.2 Total Transmission in Fiber

The total transmission is measured by integrating over all outgoing angles of light. Total transmission is defined as the total flux divided by the incident flux. Then, the total transmission found,

$$T \equiv \frac{J_{out}|_{z=L}}{S_0} = -\frac{D}{S_0}\frac{\partial I}{\partial z}|_{z=L} = \frac{l_{tr} + z_{e_1}}{L + z_{e_1} + z_{e_2}} \tag{2.26}$$

2.3 Mixing Channel

2.3.1 Scattering Channels

Throughout the scattering medium, light propagates along different paths and interference occurs destructively and constructively at the random point. The field $E(r_b)$ at the certain position r_b is calculated by summing field contributions coming from different points, r_a. The field $E(r_b)$ calculated as,

$$E(r_b) = \int G\,(r_b, r_a) S(r_a) d^3 r_a \tag{2.27}$$

Where $G(r_b, r_a)$ the non- averaged Green's function, it describes propagation of the light from the sources r_b to the r_a. This equation can use for all linear media.

2.3.2 Intensity Distribution of Speckle Pattern

A speckle pattern is a representation of the energy distribution at the end of fiber. Laser transmission leads to the a formation of speckle patterns. Light interference between the modes causes to occuring speckle patterns at the end of fiber. It looks like randomly high energy with a gap appears at the end of the fiber. As an example, one of the speckle pattern in our setup is showm in the Figure 2.3.

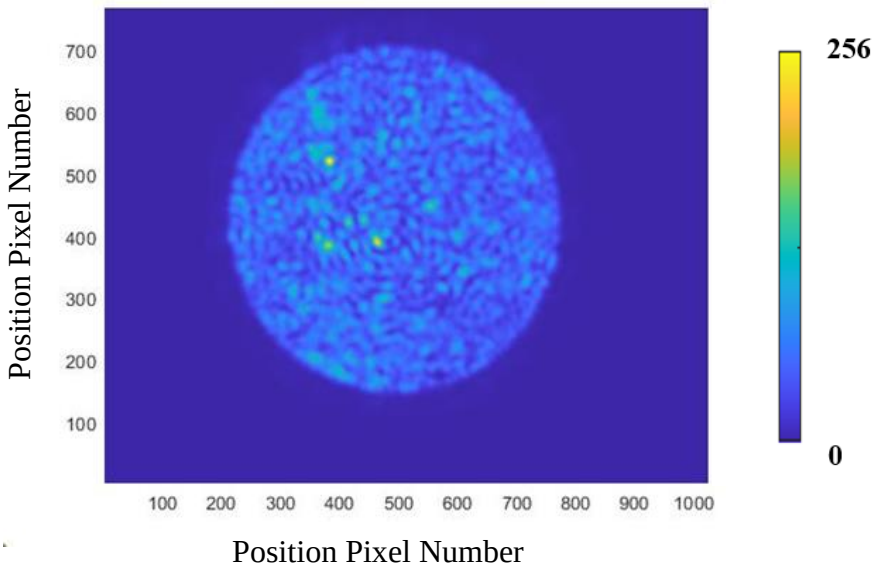

Figure 2.3 Basic speckle pattern. This is representation of the energy pattern that is appears at the end of a fiber.

The probability density function of the field modulus$|E_b|$, that is calculated by summing N independent transmission coefficients. Then we get,

$$P_{E_b}(|E_b|) = \frac{2|E_b|}{\sigma} e^{-|E_b|^2/\sigma^2} \tag{2.28}$$

The average intensity is calculated by integrating the Eq. 2.25 multiplied by$I_b \equiv |E_b|^2$,

$$\langle I_b \rangle = \int_0^\infty dE_b |E_b|^2 \, P_{E_b} = \sigma^2 \tag{2.29}$$

To calculate the intensity distribution we use Eq. 2.26 with substituting $|E_b|^2$ by I_b and introducing the Jacobian which accounts for the coordinate transform from field to intensity equal to $1/2|E_b|$. The intensity distribution measures,

$$P_{I_0}(I_b) = \frac{1}{I_0} e^{-I_b/I_0} \tag{2.30}$$

2.4 Wavefront Shaping Process

In the previous section, we explain the channel mixing process that the random scattering of light inside a scattering media. Light that travels inside the media leads to random phases and amplitudes. The mixing process inside the disordered media is quite complicate and indiscriminate. Since the reversibility of Maxwell's equations, the reverse mixing process is always valid with enhancing intensity at the desired point where the channels demix.

2.4.1 Physics Behind of Wavefront Shaping Process

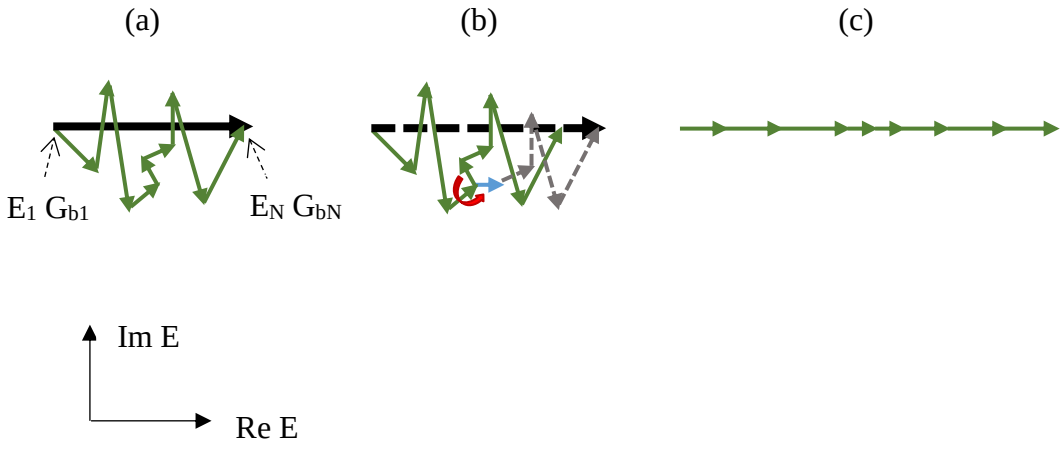

Figure 2.4 Description of channels demixing with complex amplitude representation of the field. In (a) the initial case is explained. All channels contribution is randomly at the total field. In (b) all phase are cycled to find the field transmission coefficient. The red lines and dashes line represent the adjusted phase. In (c) all phase is set to right shift since all transmission coefficient are known, all phase are in phase at the target positon.

The field at a certain point r_b is equal to the summing of the fields of the incoming scattering channels times their transmission coefficients. In a homogeneous illumination of the media the field E_b calculated as,

$$E_b = A\sum_a^N |G_{ba}|\, e^{i(\emptyset_{ba}-\emptyset_a)} \tag{2.31}$$

Where $\emptyset_{ba}$ is the phase of the transmission coefficient and $\emptyset_a$ is the phase of the light that enter the sample from the channel a. The interference pattern is changing completely while adjusting the phase of one or more channels [48].

While changing the phase of channel a, the intensity at the point r_b is calculated as,

$$I_b = I_{bg} + 2A|G_{ba}||E^*_{b\bar{a}}|\cos(\emptyset_a - \emptyset_{b\bar{a}}) \tag{2.32}$$

With,

$$E_{b\bar{a}} \equiv A\sum_{a'\neq a}^N G_{ba'}e^{i\emptyset_{a'}} \tag{2.33}$$

Where the $I_{bg} = |E_{b\bar{a}}|^2 + A^2|G_{ba}|^2$ is the background intensity with the channel a interferes Figure 2.4.

2.4.2 Maximum Intensity Enhancement

The maximum intensity that can be achieved with channel demixing is depended to the number of controllable incident channels, N. In this part, we will explain an equation for the maximum intensity enhancement, identified as the ratio between the ideal intensity and the speckle averaged intensity. The intensity at the desired point, I_b, is calculated as,

$$I_b \equiv |E_b|^2 = A^2\sum_{a=1}^N G_{ba}e^{i\emptyset_a}\sum_{a'=1}^N G^*_{ba'}\, e^{-i\emptyset_{a'}} \tag{2.34}$$

Where the A is the amplitude of the different channels.

We study the ensemble averaged intensity at the desired point. The G_{ba} is the transmission coefficients related with the circular Gaussian distribution and statistically independent [49, 50]. Hence, the ensemble averaged of G_{ba} is equal to zero, $\langle G_{ba}\rangle = 0$.

To average and rewrite the above Eq. 2.31 into sum with $a \neq a'$ and $a = a'$,

$$\langle I_b \rangle = A^2 \left[\sum_a^N \langle |G_{ba}|^2 \rangle + \sum_a^N \sum_{a \neq a'}^N \langle G_{ba} e^{i\emptyset_a} \rangle \langle G_{ba}^* e^{-i\emptyset_a'} \rangle \right] \quad (2.35)$$

The $\emptyset_a$ and $\emptyset_{a'}$ are the phase of the different incident channels. These are independent and not related with the transmission coefficients G_{ba}. The ensemble averaged sum of the cross terms with $a \neq a'$ is equal to zero. Then, the averaged intensity becomes for considering random illumination, $\langle I_{b,0} \rangle$

$$\langle I_{b,0} \rangle = A^2 N \langle |G_{ba}|^2 \rangle \quad (2.36)$$

Now, we adjust the phases for each channel to compensate for the phase retardation inside the sample; $\emptyset_a = -\emptyset_{ba}$. Therefore, all channels are in the same phase and interfere constructively at the desired position giving a maximum intensity, $I_{b,max}$

$$\langle I_{b,max} \rangle = A^2 N [\langle |G_{ba}|^2 \rangle + (N-1) \langle |G_{ba}| \rangle^2] \quad (2.37)$$

CHAPTER 3

EXPERIMANTAL SETUP

3.1 Setup

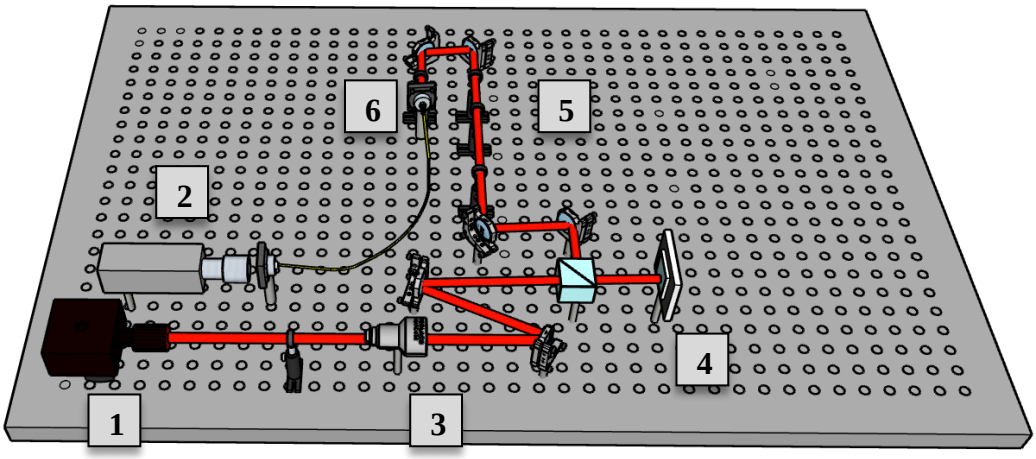

Figure 3.1 The laser emits lights (1), camera monitors the light at the end of fiber cable (2), beam expander increase the beam size (3), the SLM modulate the phase of light (4), lenses compress the light before the fiber (5), and light is coupled to the fiber cable (6).

The main experimental setup is shown in Figure 3.1. The power 100 mW and 671 nm wavelength laser light beam pass through a 10 ND filter before into the beam expander. After the beam expander light travel between two mirrors and after passing the polarizing beam splitter and incident on the SLM. Light goes to two mirrors after reflecting from the SLM surface. Then, light passes through the beam compression lenses and couples the fiber optic cable. Finally, the speckle at the end of the fiber optic cable is monitored by the camera.

The SLM and camera are controlled via a computer. The phase patterns are adjusted using algorithms that control the SLM. The SLM pixels are grouped by 30x30 pixels that are called superpixels.

3.2 Experiment

In this chapter, we present optimization algorithms created in this thesis for wavefront shaping via SLM. This experiment is based on phase modulation so the SLM device is a key element of our experiment [51]. The information about the SLM is verified by the manual [52]. The SLM has 1024x768 pixels with a pixel size of 10 μm. We managed phase retardation on each pixel with controlled the voltages applied to each pixel independently.

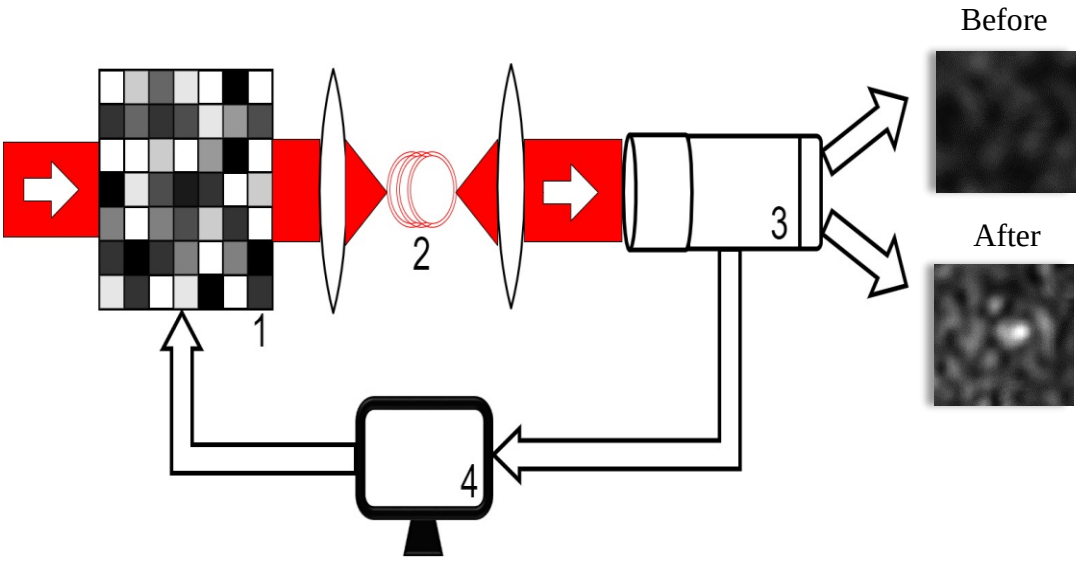

Figure 3.2 Feedback method for achieving optimization algorithms for wavefront shaping. An incident beam is shaped by SLM (1) and these shaped beam enter into optical fiber (2), a detector (3) detect the total transmitted light that reaches the target area. A feedback algorithm (4) uses the signal from the detector to program the phase modulator. Before the algorithm is started, the transmitted light forms a random speckle pattern. The algorithm changes the incident wave to increase the intensity in the target area. After a few iterations, the transmitted light focuses on the target.

The key component of optimisation via wavefront shaping setup through a multi mode fiber suing spatial light modulator is shown in Figure 3.2.

Using the algorithms that we implement/develop, we can combine neighboring pixels into one superpixel with any desired size, see Figure 3.3. Each superpixel independently allows us to modulate the phase of light [53, 54].

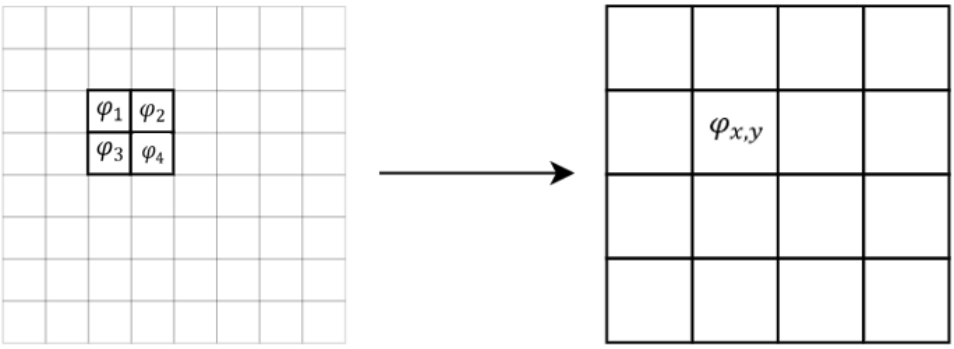

Figure 3.3 A schematic representation of the super-pixel. A single super- pixel corresponce to the 30×30 pixels.

SLM consist of 2D array pixels and they are grouped with 30 equally micro pixels square parts. Therefore, one superpixel consists of 900 micro pixels in our experiments. In literature, there are varius technique used for wavefront shaping. The most widly approtiate technique is used in this study that is independently controling phase and amplitude of a laser beam by use of a SLM. [55, 56].

We assume that the linear changes in the phase shift is the function of gray scale Figure 3.4 [57]. The Algorithms regulate the phase retardation for each superpixel individually to a value between 0 to π.

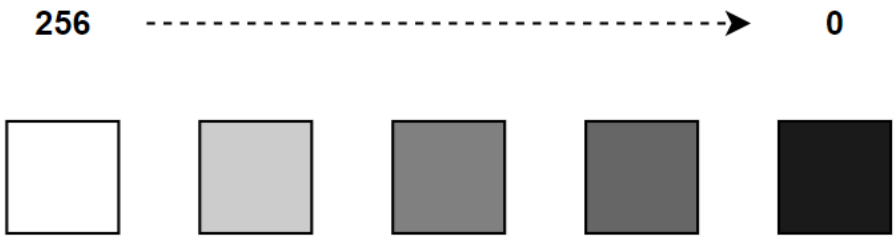

Figure 3.4 Represantation of five gray scale values that are used in algorithms.

These algorithms work based on a feedback mechanism. Before running the algorithms, all pixels values are set to 0 for all algorithms except the Monte-Carlo algorithm. These algorithms get the best configuration for phase retardation that all superpixels are in phase at the selected same 5×5 pixels for all algorithms.

In our case the scattered media is a multimode fibre cable. Light is scattered while passing through the fibre cable. Behind the fibre is a detector that supplies feedback for the algorithms. The algorithms determine the target area that the intensity is maximized. The target intensity reacts sinusoidally when the phase of the superpixel is changing. The target area at the detector is the result of all superpixels interference from scattered light at the beginning.

The performance of the all algorithms in the scattering media is quantified by the enhancement. The enhancement μ is defined as

$$\mu = \frac{I_N}{\langle I_0 \rangle} \tag{3.1}$$

Where I_N is the intensity in the desired point after optimisation, $\langle I_0 \rangle$ is the total averaged transmitted intensity before optimisation. In a smoothly stable system, enhancement is directly proportional to N, this means that increasing the number of scanning groups in a certain area allows for more shaping incident wavefront. Its results with the boosted intensity at the target. However, there is a limit for number

of iteration that can be measured. Longer measurements than 3 hours are not preferred since after this duration the setups starts to drift.

Here, we will present four base algorithms and 3 hybrid version of them. The advantages and disadvantages of these algorithms are explained, and they will be analysed in detail.

3.2.1 Optimization Algorithms for Focusing Light through Turbid Media

3.2.1.1 Monte Carlo Algorithm

The Monte Carlo algorithm is differ from the stepwise, continuous and segmented algorithms. The whole superpixels are scanned with different way in these algorithms.

The Monte Carlo algorithm changes the value of all superpixels in each iteration [58]. Therefore, the effect of each iteration is much more apparent than the stepwise, continuous, and segmented algorithms Figure 3.5.

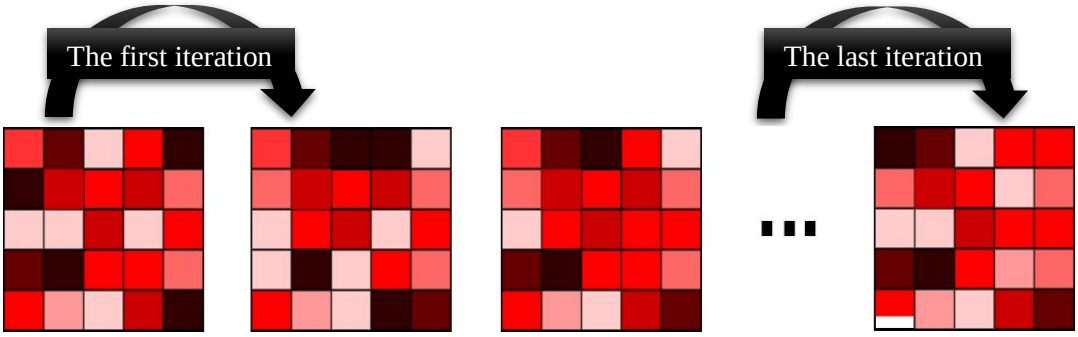

Figure 3.5 Monte Carlo algorithm, variables in Eq. 3.2 except x and y are created randomly for each iteration and the SLM is updated after each iteration.

Let $\emptyset_n$ is the phase value at the n^{th}. In order to calculate the phase for the next iteration, a previous phase,$\emptyset_p$ is calculated as

$$\emptyset_p(x,y) = \arg[(1-\epsilon)\, e^{i\emptyset_n(x,y)} + \epsilon e^{i(kx\cos\alpha + ky\sin\alpha + \theta)}] \qquad (3.2)$$

where x and y are the coordinates of the SLM pixels, and random variables are generated for all other variables at each iteration. ϵ is generated between [0, 1/2], k is generated from $[0,k_{max}]$ where k_{max} calculated from the setup parameters as explain in [56]. The phase $\emptyset_n$ is updated to $\emptyset_p$ if the performance is improved, meaning that target intensity is higher than $I_p^{target} > I_n^{target}$ previous intensity. Otherwise, there is no update, the $\emptyset_p$ is calculated again with new random value Figure 3.6. The operation time is selected the same as the other algorithms' time to make a comparison.

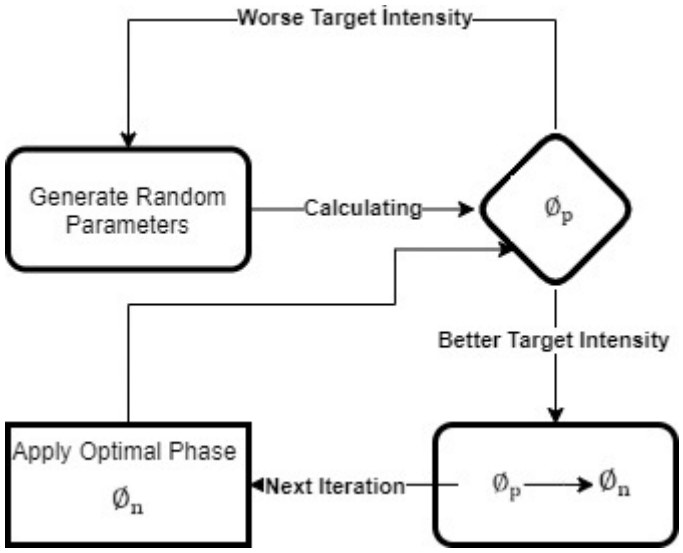

Figure 3.6 Monte Carlo Algorithm Diagram

The hybrid version is formed by combining the Monte Carlo algorithm and continuous algorithm. The Monte Carlo algorithm is worked a certain time and one continuous algorithm is run right after the Monte Carlo completed.

3.2.1.2 The Continuous Sequential Algorithm

The continuous sequential algorithm is based on starting with all superpixels are in phase at SLM initially. This means that optimum wavefront can be constructed by optimizing each of the superpixels separately. The computer consecutively scan the phase of each of the 30 superpixels from 0 to π. The phase of each superpixel where the target intensity is maximum according to the feedback signal is directly set after each measurement Figure 3.7.

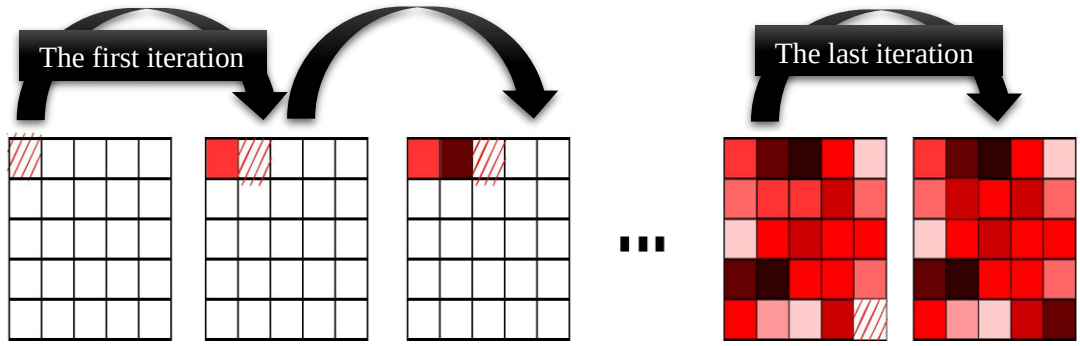

Figure 3.7 The continuous sequential algorithm, all segment are addressed sequentially, after the optimal phase is determined for each superpixels, the SLM is updated after each iteration (red squares).

3.2.1.3 The Stepwise Sequential Algorithm

The stepwise sequential algorithm is very similar to the continuous sequential algorithm except the phase retardation of each superpixel is adjust to 0 before continuing with the next superpixel. In this way, the background field of the SLM does not change. Only after all iteration are completed, the recorded maximal phase of each superpixel is set. Now, all superpixels have same phase as the original background field Figure 3.8.

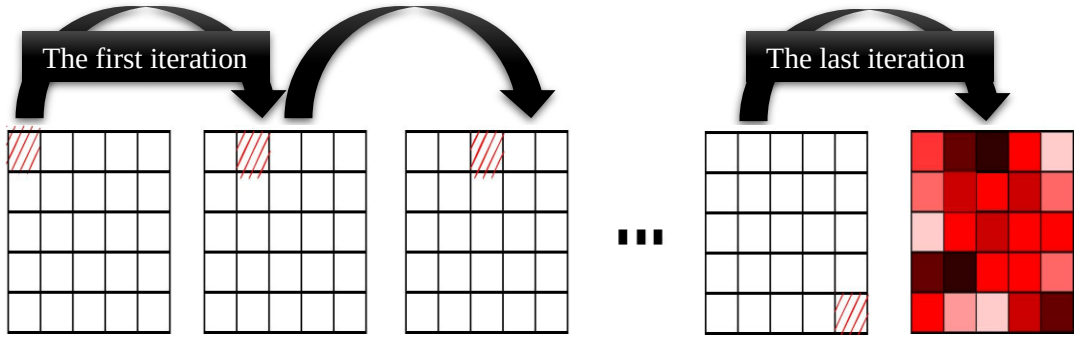

Figure 3.8 The stepwise sequential algorithm, after the optimal phase is determined for all superpixels, the SLM is updated to construct the optimal wavefront.

3.2.1.4 The Segmented Algorithm

The segmented algorithm is different from the continuous and stepwise algorithms. These algorithms scan the all superpixel consecutively between from 0 to π. However, the segmented algorithm changes the phase of random selected superpixel and directly set to its maxımum value after each measurement Figure 3.9.

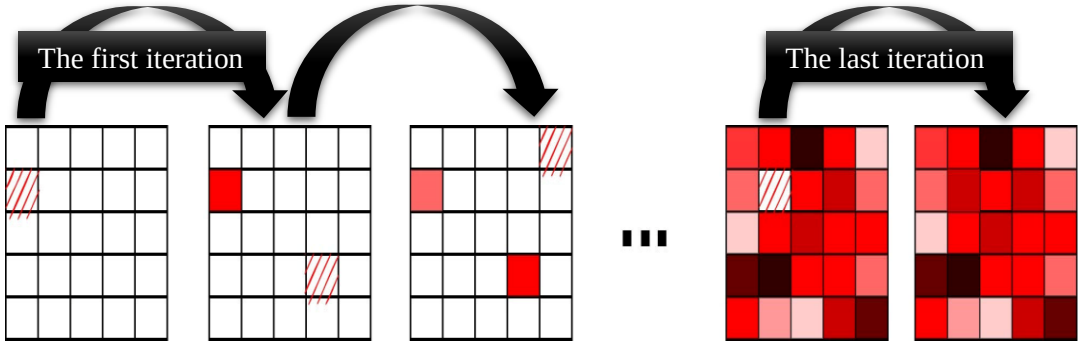

Figure 3.9 The segmented algorithm, randomly selects of one of superpixels and adjusts their optimal phase, the SLM is updated after each iteration.

3.2.1.5 Hybrid 1 Stepwise Continuous Algorithm

The hybrid version is formed by combining two step stepwise algorithm and one step continuous algorithm. The two stepwise algorithms are worked first, and one continuous algorithm is run right after two stepwise completed.

3.2.1.6 Hybrid 2 Segmented Continuous Algorithm

The hybrid version is formed by combining two step segmented algorithms and one step continuous algorithm. The two-segmented algorithms are worked first, and one continuous algorithm is run right after the two segmented completed.

CHAPTER 4

RESULTS AND DISCUSSION

4.1 Phase Control Algorithms for Focusing Light

In this chapter, we present four different optimization algorithms and three hybrid version which arise from combination of indiviual alorithms for creating a wavefront that focus light through a multimode fiber. We analyse these algorithms according to their dynamic behaviour and compare their performance with respect to each other. These performance criteria are; the **speed** to reach the threshold improvement, the **total enhancement** at the speckle pattern and the **regional enhancement** at the desired point. In the following part, we are going to show the data and figures with the processed different phase control algorithms.

4.1.1 Speed of Six Phase Control Algorithms

In this section, we present four base algorithms and their speed as well as how the hybridized combination of these algorithms affect the speed while focussing light through a multimode fiber.

The speed is calculated by number of iterations divided by the elapsed time. The SLM has resolution 1024×768 pixels, super pixel method is used in the experiment. One super pixel is created from 30×30 pixels and one super pixel is scanned in five sections between 0 to π. Therefore, one step scan of whole system is equal to;

$$\mathrm{K} = \frac{(1024\times768)}{30\times30} \times 5 = 4369 \tag{4.1}$$

K is iteration number, 1024x768 is the pixel number on the SLM, and 900 is the super pixel number. Our experiment took place three complete repetitions so that number of iteration for our system is;

$$K = \frac{(1024 \times 768)}{900} \times 5 = 4369$$

$$K \times 3 = 13107$$

This calculation is not valid for hybrid Monte Carlo-Continuous algorithm and its pure version (Monte Carlo algorithm) since another phase modulation formulation is used to perform this method. There are no specific complete repetitions in the Monte Carlo algorithms as with other algorithms. The iterations is created changing the variables from the eq. 3.2. The last iteration is chosen after the visible focussing formation at the target point. The iteration number is quite bigger than others since reaching the threshold value for focusing took longer time. There is a visible focussing formation at the approximately 28500 iteration number for Monte Carlo algorithm.

We concluded that continuous, stepwise and segmented algorithms have almost same operation time and same final enhancement. However, these three algorithms have different way to accomplish its target. The results of three algorithms are shown in Figure 4.1.

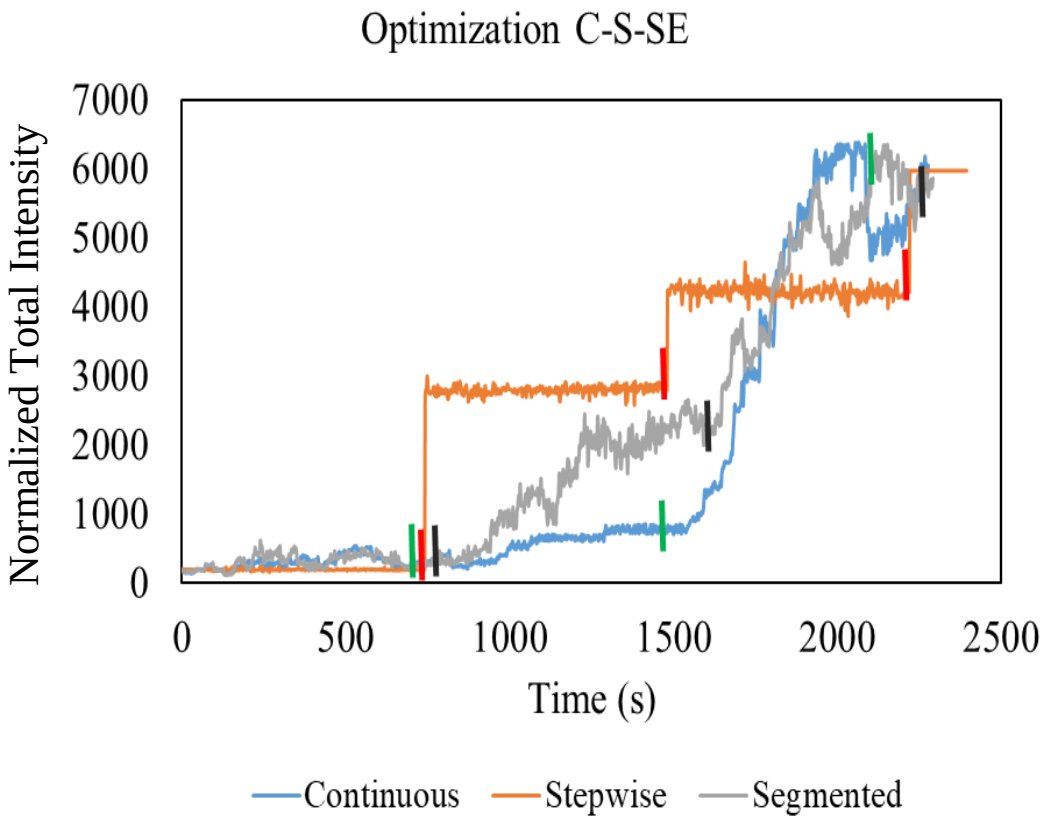

Figure 4.1 Time versus enhancement of the continuous, stepwise and segmented algorithms, the green, red and black rods are the complete repetition point of continuous.

The three algorithms are created using different technique so there is time difference betwen each data set. The iteration time and the time for three complete repetitions are shown in the below Table 1. One iteration time is calculated as;

$$\text{One repetition time} = \frac{\text{total time}}{\text{total iteration number}}$$

Table 1 Show the three algorithms single iteration times,complete repetition times and total operation times

Algorithms Type	**One iteration time (s)**	**Complete repetition time (s)**	**Repetition**	**Total time (s)**
Continuous	0.183	799	3	2273
Stepwise	0.188	821	3	2335
Segmented	0.193	843	3	2397

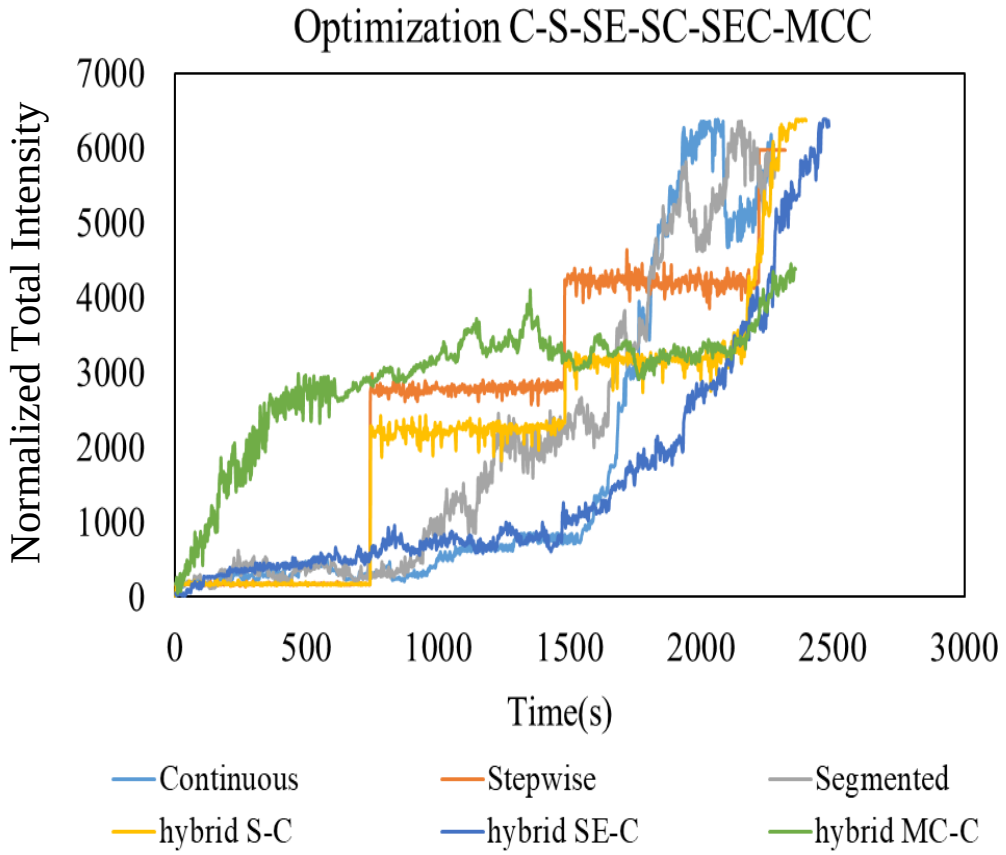

Figure 4.2 Time versus enhancement of six algoritmhs.

Six different type of optimization methods based on four algorithms are examined in this study. These are continuous, stepwise, segmented, hybrid S-C, hybrid SE-C and hybrid Monte Carlo –C methods. The speeds of six methods are elapsed time from

start to when clear visible focus occurs at the target point. The visible focus value is chosen as 5000 intensity in the 5x5 pixels at the target area, the worst performance have considered when choosing this value Figure 4.2. The results are shown in the Table 2.

Table 2 Show the total elapsed time and iteration number until the visible focus formation

Type	Total Time (s)	Iteration Number
1. Continuous	1850	10278
2. Segmented	1856	10311
3. Stepwise	2221	12342
4. Hybrid S-C	2233	12408
5. Hybrid SE-C	2489	13844
6. Hybrid MC-C	2706	15036

The continuous algorithm has reached the threshold value faster than the others. Segmented algorithm have almost same performance with continuous, stepwise has 20% lower speed than the continuous. The hybrid MCC has the worst performance with 46% lower speed than the continuous.

However, there is a time interval at the beginning of the experiment where the hybrid MC-C algorithm have great performance that increase the initial value by 150 times. Focal point have clearly seen after the 350 second of the experiment, see Table 4. In the same time interval, there is no any focal point at the other methods see The 2500 intensity in the 5×5 pixels at the target area is chosen since there is a meaningful data for focussing light. The ranking and detail information is shown in the below Table 3.

Table 3 Show the performance of six algorithms at the beginning

Type	Time (second)	Iteration Number	Intensity Value
1. Hybrid MC-C	357	180	2722
2. Stepwise	743	374	2720
3. Hybrid S-C	744	375	2734
4. Segmented	1526	768	2690
5. Continuous	1687	849	2663
6. Hybrid P-C	2146	1080	2652

Hybrid MC-C is 601% faster than the continuous method that is the slowest methods amongst others and 208% faster than the stepwise methods that is the fastest methods amongst others.

There is a visible focal point at time 357 for hybrid Monte Carlo – C algorithm. However, the focal point formation have taken more time for others. All algorithms target point at the time 357 second are shown in the below Table 4.

Table 4 Show the screenshot of each algorithm at 357 seconds

Algorithms	Focal Point at the same time (357s)
Hybrid MC-C	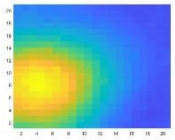
Stepwise	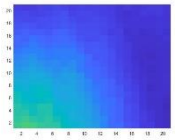
Hybrid S-C	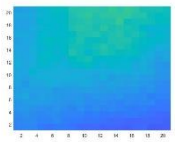

Table 4 (continued)

Algorithms	Focal Point at the same time (357s)
Segmented	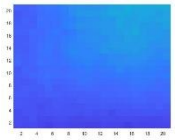
Continuous	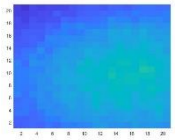
Hybrid P-C	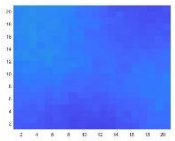

4.1.2 Enhancement of Six Phase Control Algorithms

In this part, regional enhancement and total enhancement of six algorithms are present.

Random point is chosen in the speckle pattern to focus light with size 5×5 pixels. The chosen point coordination is 420(x) and 650(y). Regional enhancement is the intensity increasing in this sum of 5×5 pixels. The total enhancement is the intensity increasing in sum of whole 1024×768 pixels figure.

4.1.2.1 Regional Enhancement

Regional enhancement is calculated by subtracting the sum of the total selected 5×5 pixels in the speckle pattern after optimization from before optimization.

5×5 pixels size is chosen to focus light in the same coordination for all algorithms.

Before all algorithms run, pre-optimization is completed with 100×100 super pixels. This pre-optimization takes 20.5 seconds. The reasons for the requirement of pre-

optimization are diminishing the background effect and clearly seeing and compering focussing light.

In the following part, the six algorithms outcome is present.

4.1.2.1.1 Monte Carlo – Continuous Algorithm

In the hybrid Monte Carlo - Continuous algorithm, the total 12420 iterations are performed that means the Monte-Carlo algorithm ran certain time and one continuous algorihms ran one time consecutively. These algorithms completed all iterations in the 2390 seconds.

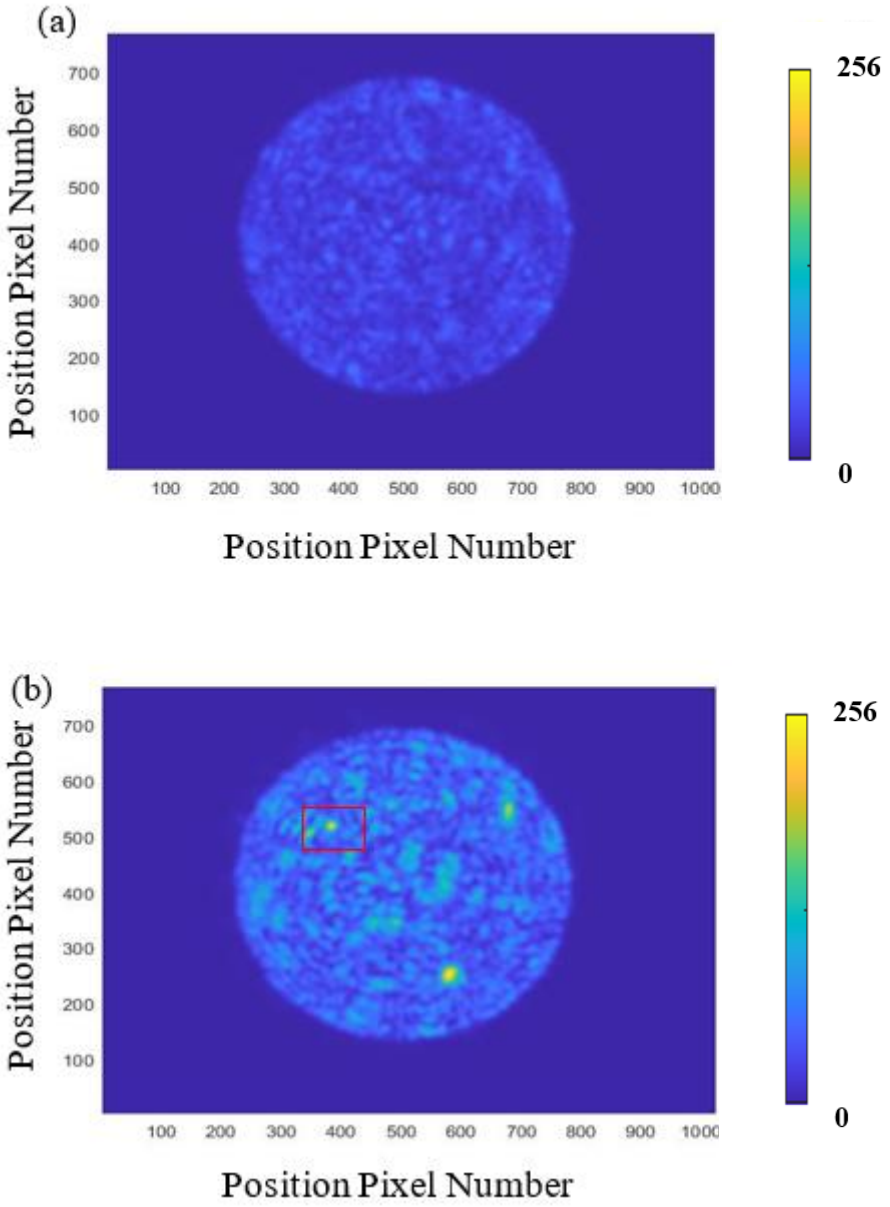

Figure 4.3 Tranmission intensity distribution through a fiber optic cable, (a) Transmission before optimisation with unshaped wavefront, all pixels have low intensity, (b) Transmission after optimisation with shaped wavefront, the selected point is highlighted in a red square. The transmission after optimisation in the selected point is 318 times brighter than the before optimisation.

The intensity value of the target 5×5 pixels area before the optimization is 20 in gray scale. One pixel average value is 0.8 of the target pixels that means all pixels have extremely low intensity. After certain time Monte-Carlo algorithm and one continuous algorithm ran consecutively, the intensity value of the target 5×5 pixels area reached to 5586. This means that transmission after optimisation is 279 times bigger than before optimisation. One pixel average value of the target pixels increased from 0.8 to 224.

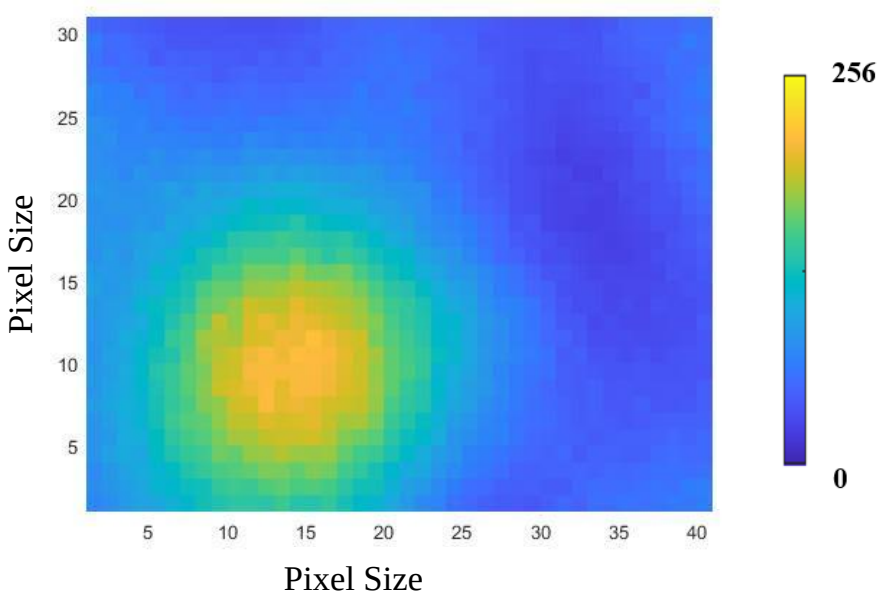

Figure 4.4 The target 5×5 pixels area in the fiber cable. After optimisation, scattered light is focussed at the target with shaped wavefront.

The target 5×5 pixels cross-section is measured for make sure that the no saturation in the pixels. There is no saturation at the target point since the intensity value does not exceed 1.

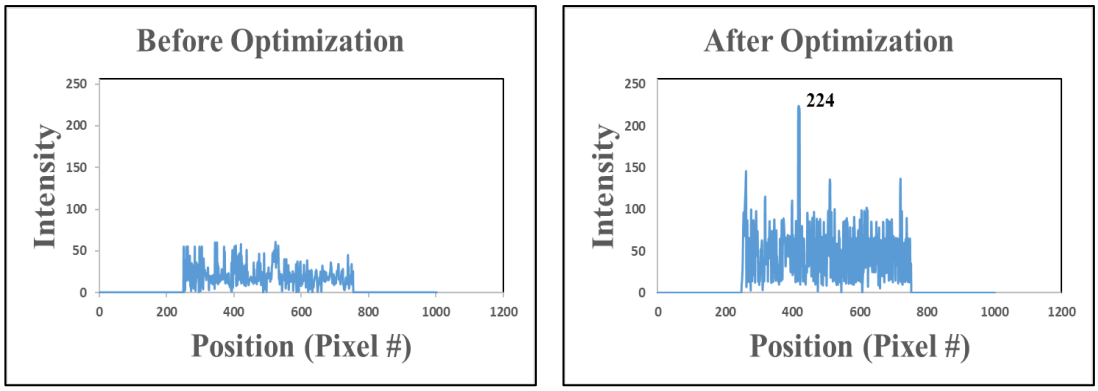

Figure 4.5 The cross section of the target point. (a) all pixels intensity before optimisation, (b) all pixels intensity after optimisation, target point pixels did not exceed the 256.

4.1.2.1.2 Continuous Algorithm

In the continuous algorithm, the total 12420 iterations are performed that means the continuous sequantial algorithms ran three times consecutively. The algorithm completed all iterations in the 2273 seconds.

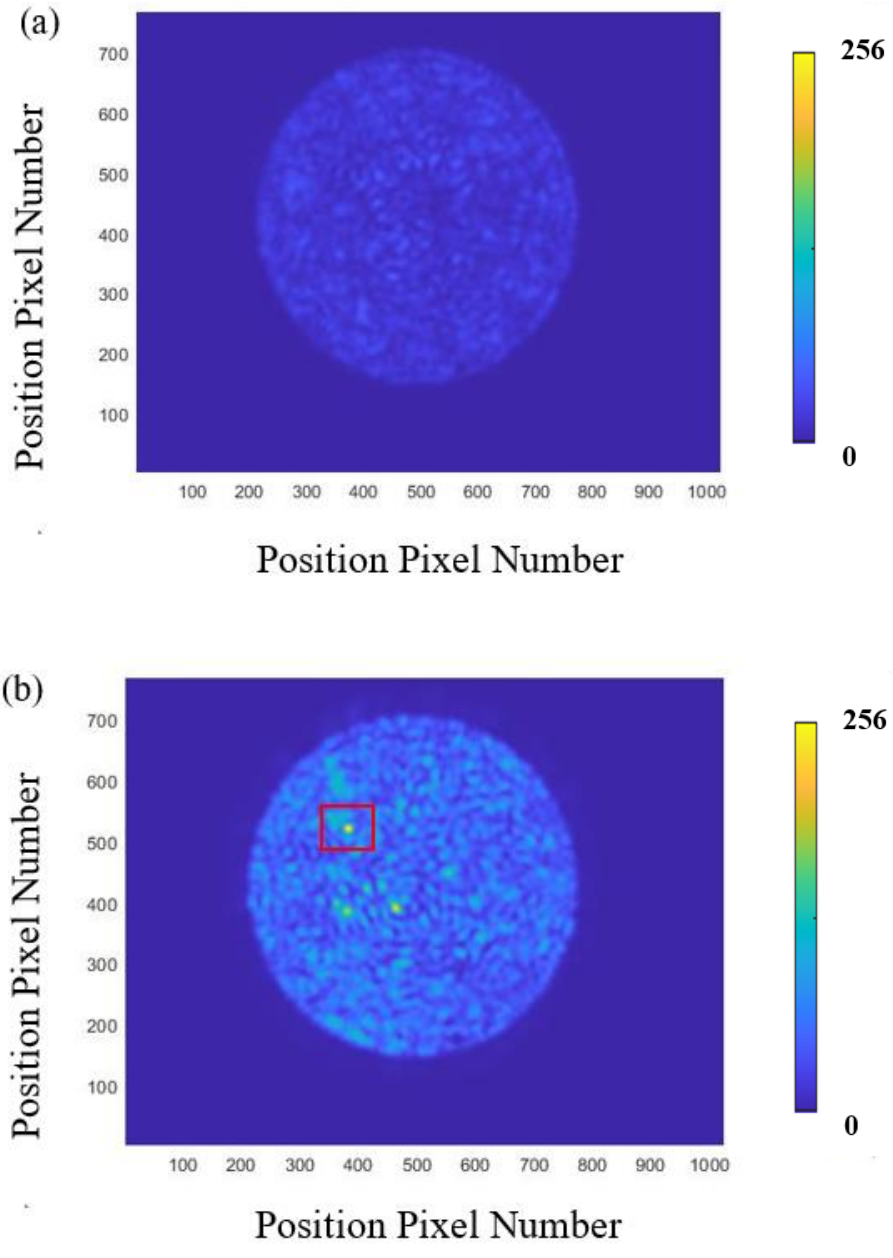

Figure 4.6 Tranmission intensity distribution through a fiber optic cable, (a) Transmission before optimisation with unshaped wavefront, all pixels have low intensity, (b) Transmission after optimisation with shaped wavefront, the selected point is highlighted in a red square. The transmission after optimisation in the selected point is 301 times brighter than the before optimisation.

The intensity value of the target 5×5 pixels area before the optimization is 20 in gray scale. One pixel average value is 0.8 of the target pixels that means all pixels have extremely low intensity. After the continuous sequantial algorithms ran three times consecutively, the intensity value of the target 5×5 pixels area reached to 6037. This means that transmission after optimisation is 301 times bigger than before optimisation. One pixel average value of the target pixels increased from 0.8 to 241.

After optimisation, light is focused in the fiber to the target pixels with wavefront shaping. In the target pixels, the highest pixel value is 249. Therefore, there is no saturation since none of pixels value above 256.

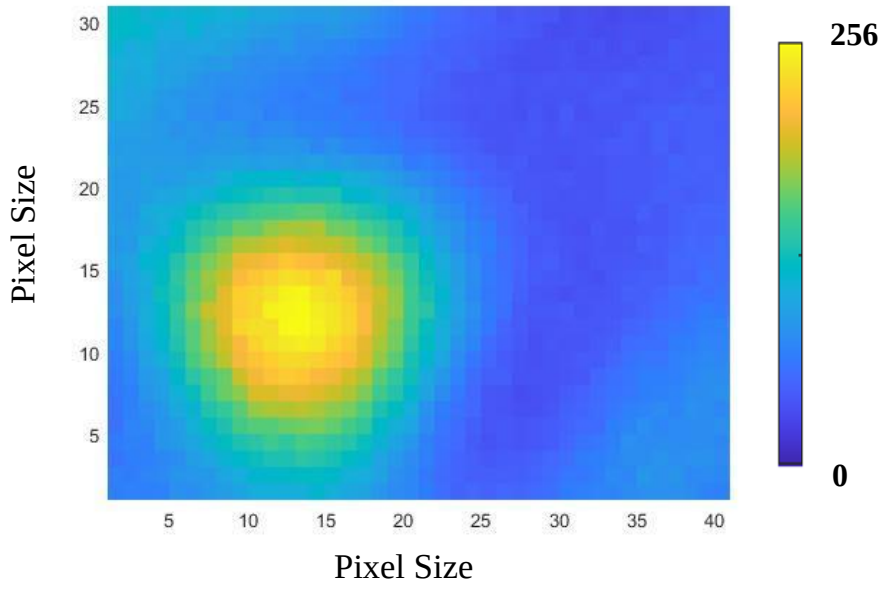

Figure 4.7 The target 5×5 pixels area in the fiber cable. After optimisation, scattered light is focussed at the target with shaped wavefront.

The target 5×5 pixels cross-section is measured for make sure that the no saturation in the pixels. There is no saturation at the target point since the intensity value does not exceed 256.

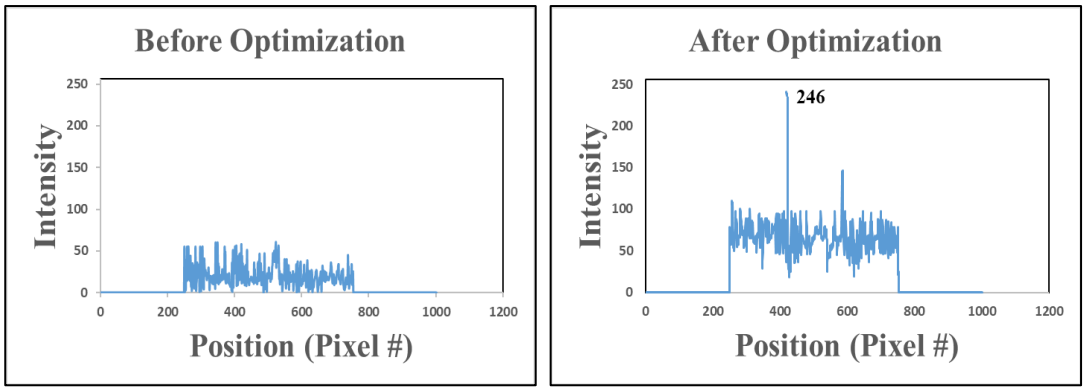

Figure 4.8 The cross section of the target point. (a) all pixels intensity before optimisation, (b) all pixels intensity after optimisation, target point pixels did not exceed the 256.

4.1.2.1.3 Stepwise Algorithms

In the stepwise sequential algorithm, the total 12420 iterations are performed that means the stepwise sequantial algorithms ran three times consecutively. The algorithm completed all iterations in the 2335 secondss.

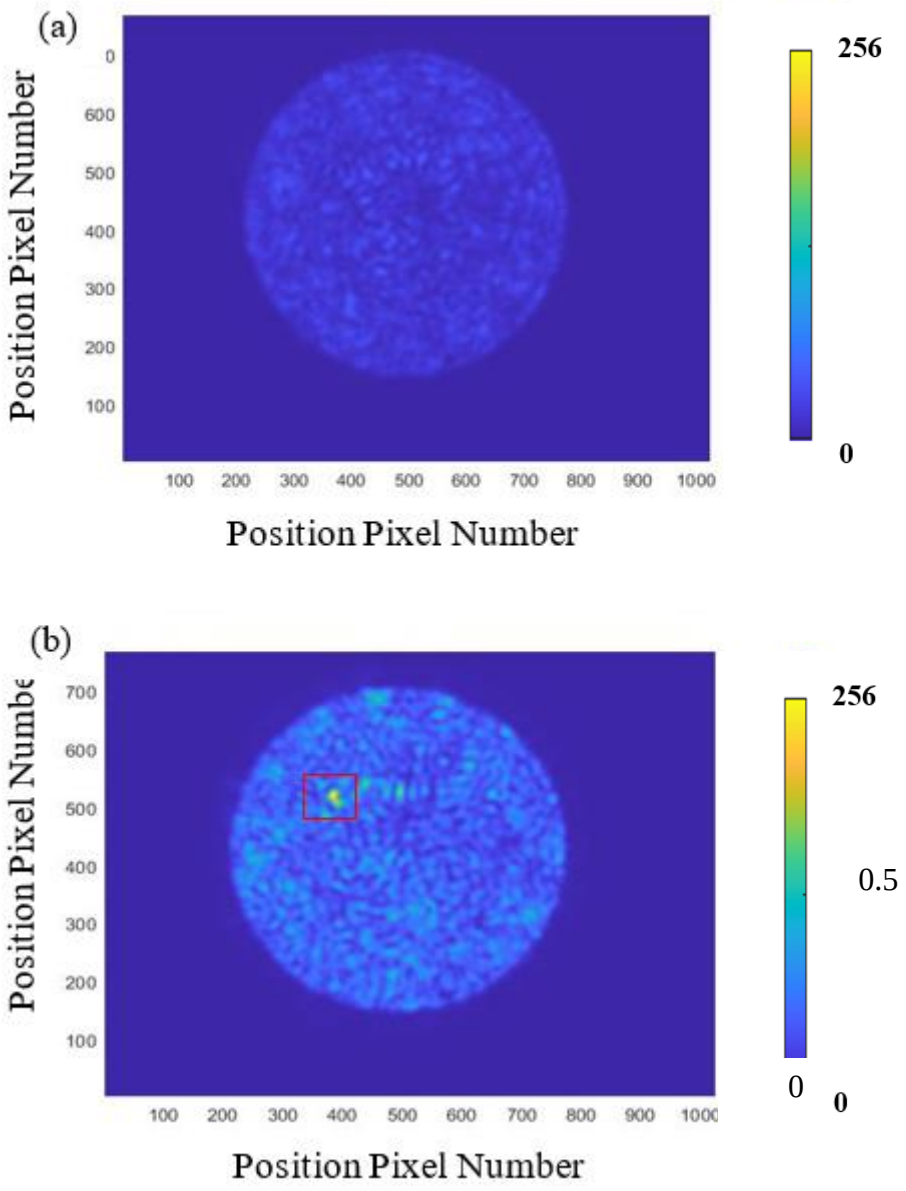

Figure 4.9 Tranmission intensity distribution through a fiber optic cable, (a) Transmission before optimisation with unshaped wavefront, all pixels have low intensity, (b) Transmission after optimisation with shaped wavefront, the selected point is highlighted in a red square. The transmission after optimisation in the selected point is 298 times brighter than the before optimisation.

The intensity value of the target 5×5 pixels area before the optimization is 20 in gray scale. One pixel average value is 0.8 of the target pixels that means all pixels have extremely low intensity. After the stepwise sequantial algorithms ran three times consecutively, the intensity value of the target 5×5 pixels area reached to 5969. This means that transmission after optimisation is 298 times bigger than before optimisation. One pixel average value of the target pixels increased from 0.8 to 239.

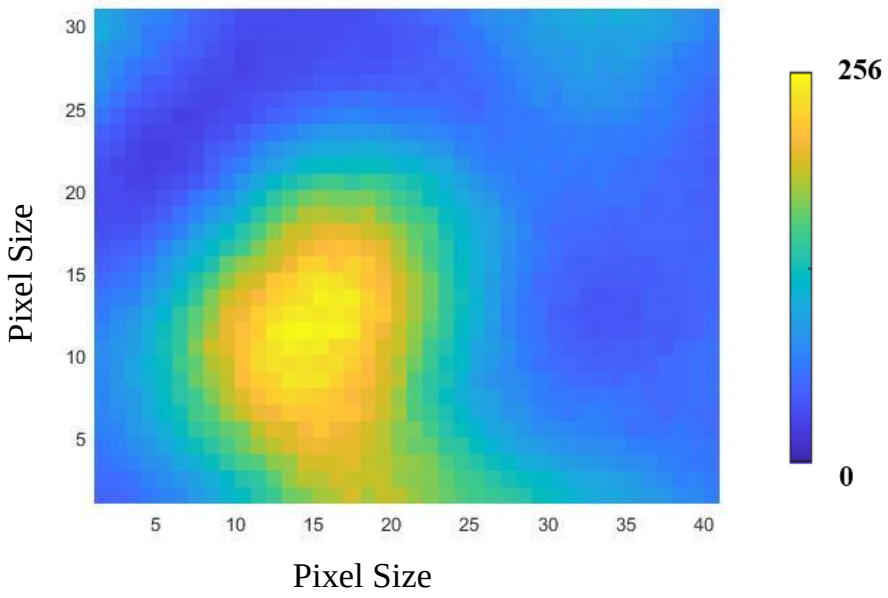

Figure 4.10 The target 5×5 pixels area in the fiber cable. After optimisation, the light is focussed at the target with shaped wavefront.

The target 5×5 pixels cross-section is measured for make sure that the no saturation in the pixels. There is no saturation at the target point since the intensity value does not exceed 256.

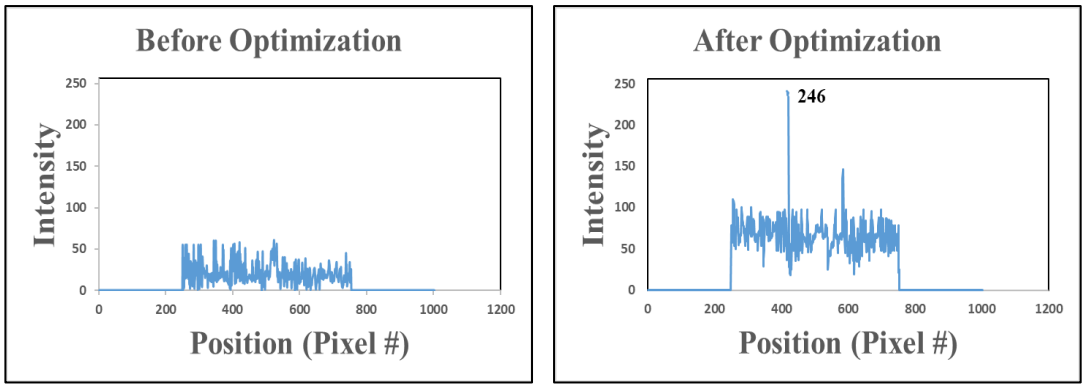

Figure 4.11 The cross section of the target point. (a) all pixels intensity before optimisation, (b) all pixels intensity after optimisation, target point pixels did not exceed the 256.

4.1.2.1.4 Segmented Algorithms

In the segmented algorithm, the total 12420 iterations are performed that means the segmented algorithm ran three times consecutively. The algorithm completed all iterations in the 2397 seconds.

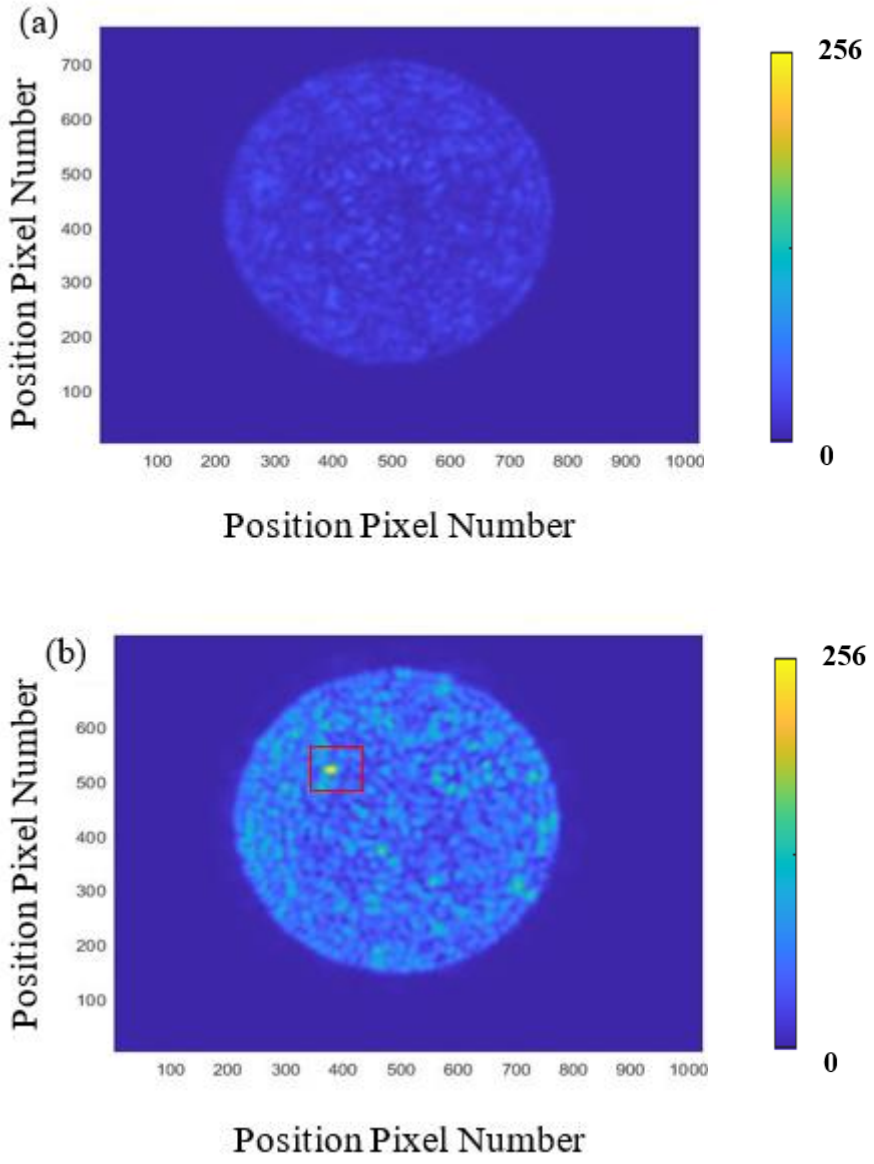

Figure 4.12 Tranmission intensity distribution through a fiber optic cable, (a) Transmission before optimisation with unshaped wavefront, all pixels have low intensity, (b) Transmission after optimisation with shaped wavefront, the selected point is highlighted in a red square. The transmission after optimisation in the selected point is 293 times brighter than the before optimisation.

The intensity value of the target 5×5 pixels area before the optimization is 20 in gray scale. One pixel average value is 0.8 of the target pixels that means all pixels have

extremely low intensity. After the segmented algorithm ran three times consecutively, the intensity value of the target 5×5 pixels area reached to 5862. This means that transmission after optimisation is 293 times bigger than before optimisation. One pixel average value of the target pixels increased from 0.8 to 237.

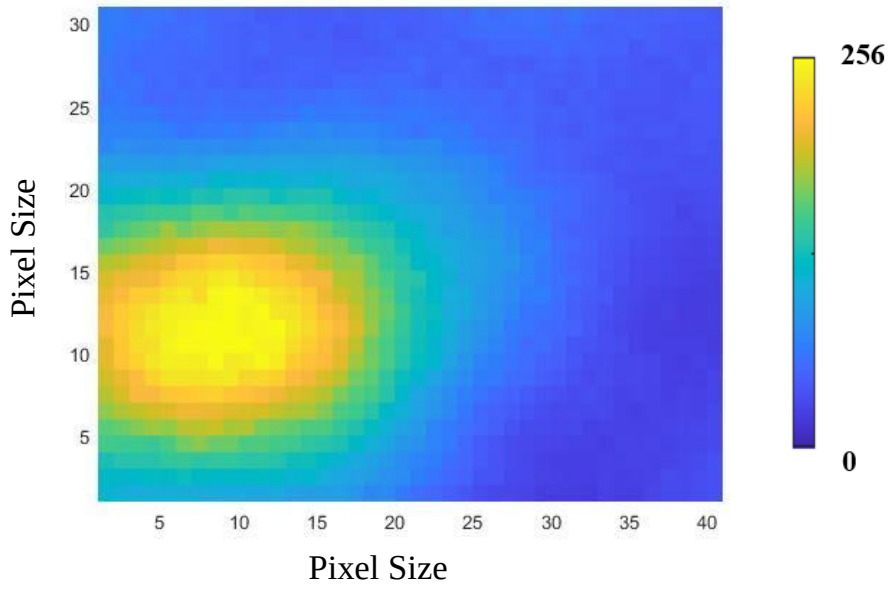

Figure 4.13 The target 5×5 pixels area in the fiber cable. After optimisation, scattered light is focussed at the target with shaped wavefront.

The target 5×5 pixels cross-section is measured for make sure that the no saturation in the pixels. There is no saturation at the target point since the intensity value does not exceed 256.

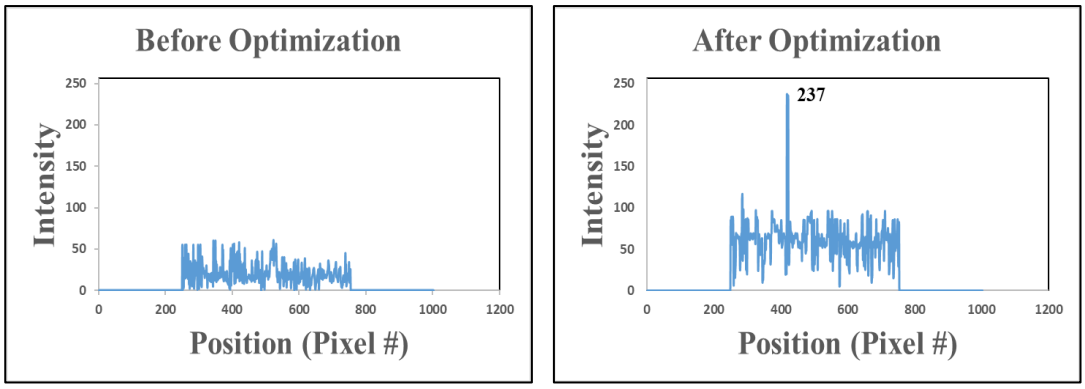

Figure 4.14 The cross section of the target point. (a) all pixels intensity before optimisation, (b) all pixels intensity after optimisation, target point pixels did not exceed the 256.

4.1.2.1.5 Hybrid Step-Con Algorithm

In the hybrid stepwise-constinuose algorithm, the total 12420 iterations are performed that means the stepwise algorithm ran two times and one continuous algorihms ran one time consecutively. These algorithms completed all iterations in the 2397 seconds.

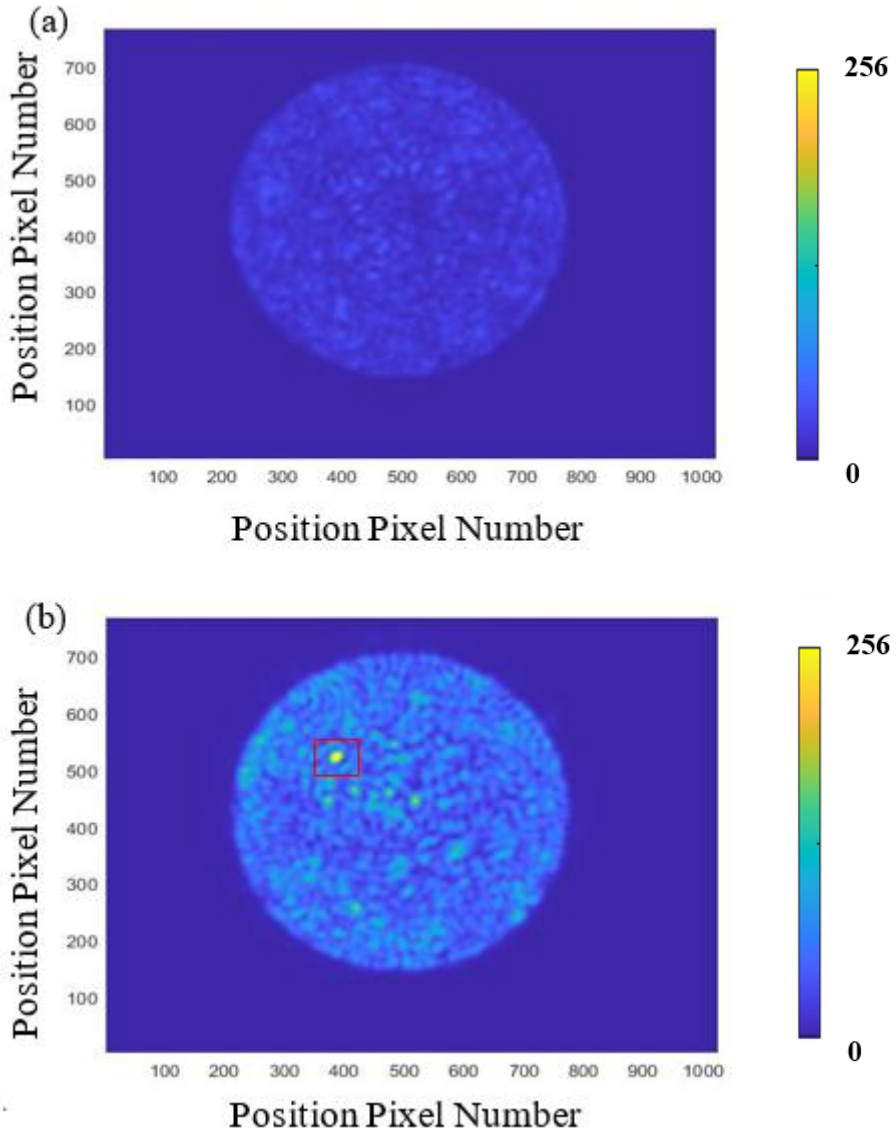

Figure 4.15 Tranmission intensity distribution through a fiber optic cable, (a) Transmission before optimisation with unshaped wavefront, all pixels have low intensity, (b) Transmission after optimisation with shaped wavefront, the selected point is highlighted in a red square. The transmission after optimisation in the selected point is 318 times brighter than the before optimisation.

The intensity value of the target 5×5 pixels area before the optimization is 20 in gray scale. One pixel average value is 0.8 of the target pixels that means all pixels have

extremely low intensity. After two stepwise and one continuous algorithm ran total three times consecutively, the intensity value of the target 5×5 pixels area reached to 6369. This means that transmission after optimisation is 318 times bigger than before optimisation. One pixel average value of the target pixels increased from 0.8 to 254.

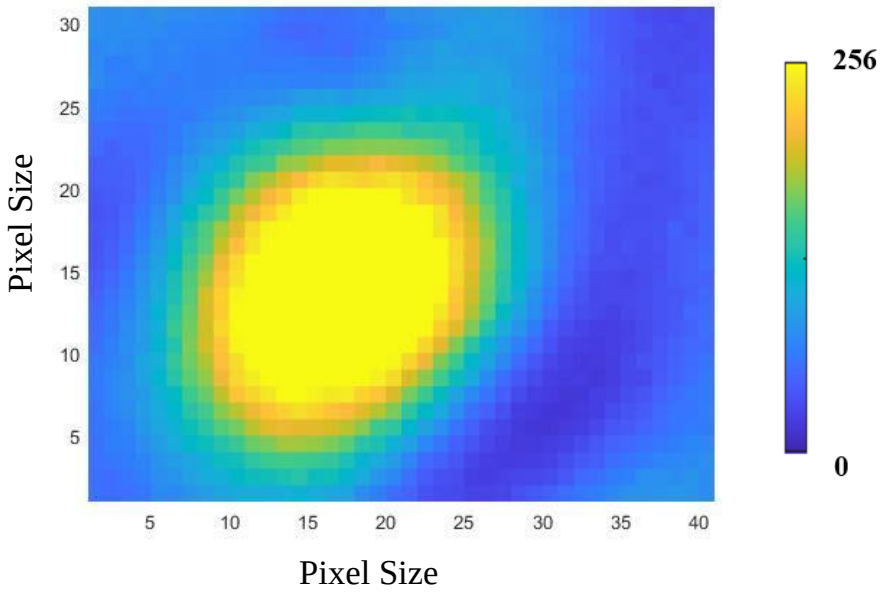

Figure 4.16 The target 5×5 pixels area in the fiber cable. After optimisation, scattered light is focussed at the target with shaped wavefront.

The target 5×5 pixels cross-section is measured for make sure that the no saturation in the pixels. There is no saturation at the target point since the intensity value does not exceed 1.

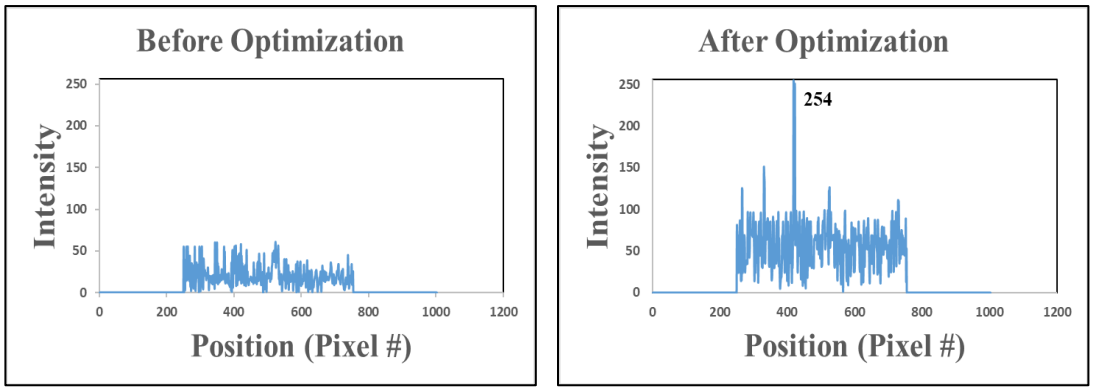

Figure 4.17 The cross section of the target point. (a) all pixels intensity before optimisation, (b) all pixels intensity after optimisation, target point pixels did not exceed the 1.

4.1.2.1.6 Hybrid Seg-Con Algorithm

In the hybrid segmented-continuous algorithm, the total 12420 iterations are performed that means the segmented algorithm ran two times and one continuous algorihms ran one time consecutively. These algorithms completed all iterations in the 2390 seconds.

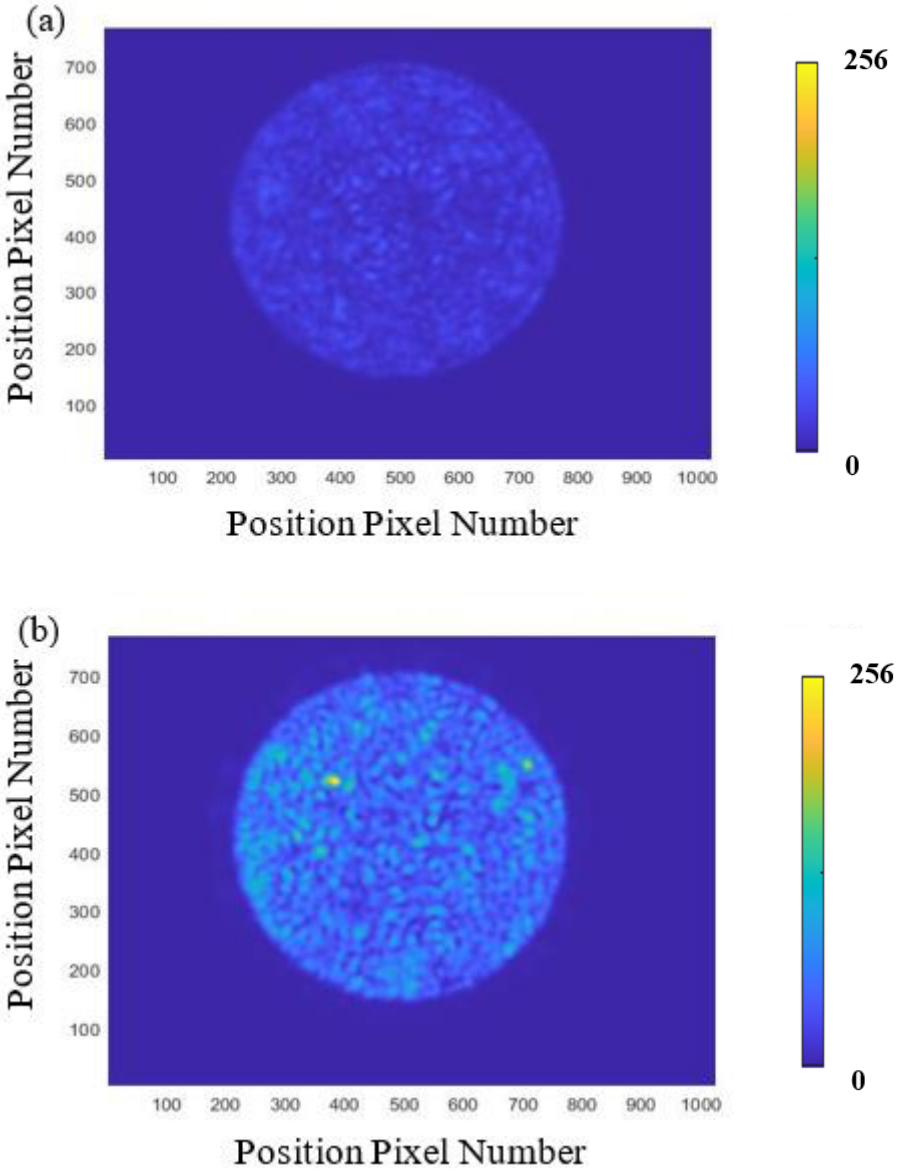

Figure 4.18 Tranmission intensity distribution through a fiber optic cable, (a) Transmission before optimisation with unshaped wavefront, all pixels have low intensity, (b) Transmission after optimisation with shaped wavefront, the selected point is highlighted in a red square. The transmission after optimisation in the selected point is 318 times brighter than the before optimisation.

The intensity value of the target 5×5 pixels area before the optimization is 20 in gray scale. One pixel average value is 0.8 of the target pixels that means all pixels have

extremely low intensity. After two segmented and one continuous algorithm ran total three times consecutively, the intensity value of the target 5×5 pixels area reached to 6219. This means that transmission after optimisation is 311 times bigger than before optimisation. One pixel average value of the target pixels increased from 0.8 to 249.

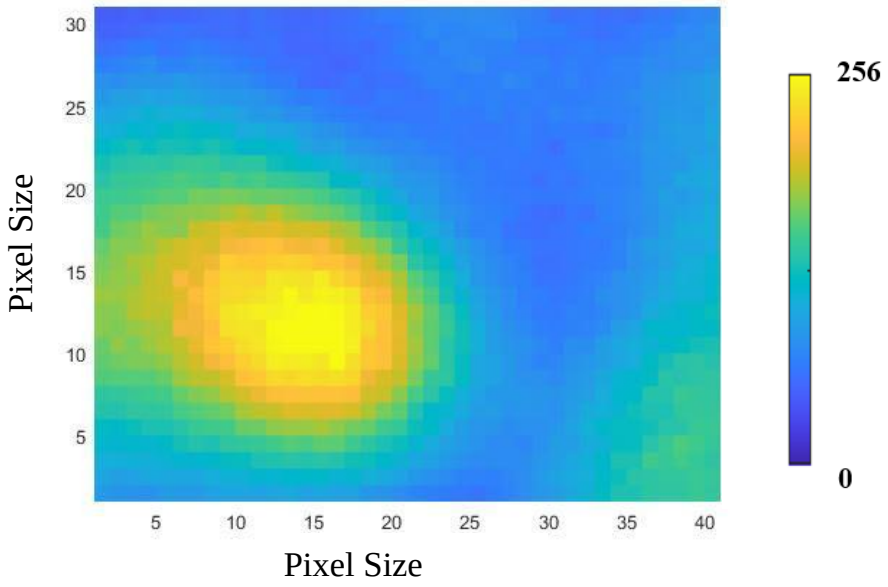

Figure 4.19 The target 5×5 pixels area in the fiber cable. After optimisation, scattered light is focussed at the target with shaped wavefront.

The target 5×5 pixels cross-section is measured for make sure that the no saturation in the pixels. There is no saturation at the target point since the intensity value does not exceed 249.

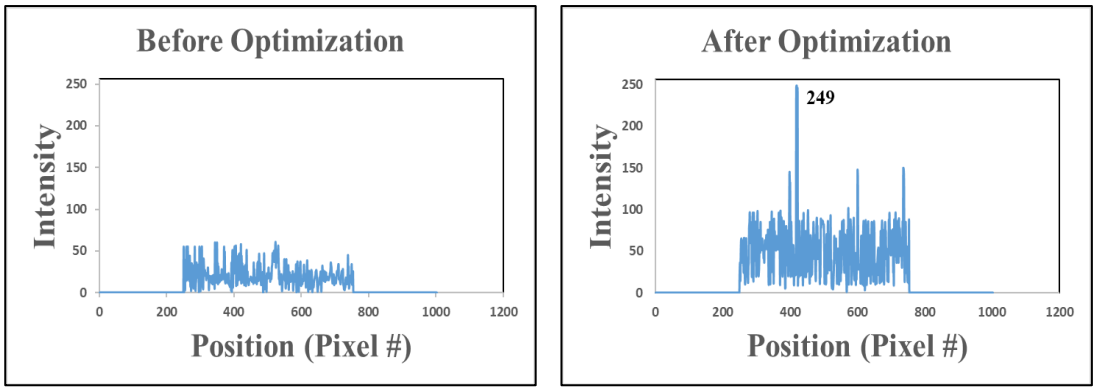

Figure 4.20 The cross section of the target point. (a) all pixels intensity before optimisation, (b) all pixels intensity after optimisation, target point pixels did not exceed the 256.

Regional enhancement of six algoritmhs are present in the below Figure 4.21. The SC has the best performance amongst others. Except the MCC, other algorithms have the similiar performance. However, the MCC has the best performance at the first period.

Table 5 Show the summary of the regional enhancement of six algorithms

Type	Initial Value	Final Value	Enhancement (times)
1. Hybrid SC	20	6369	318
2. Hybrid SEC	20	6219	311
3. Continuous	20	6037	301
4. Stepwise	20	5969	298
5. Segmented	20	5862	293
6. Hybrid MCC	20	5586	279

Increasing regional enhancement according to number of iteration during the experiment is shown in the Figure 4.21.

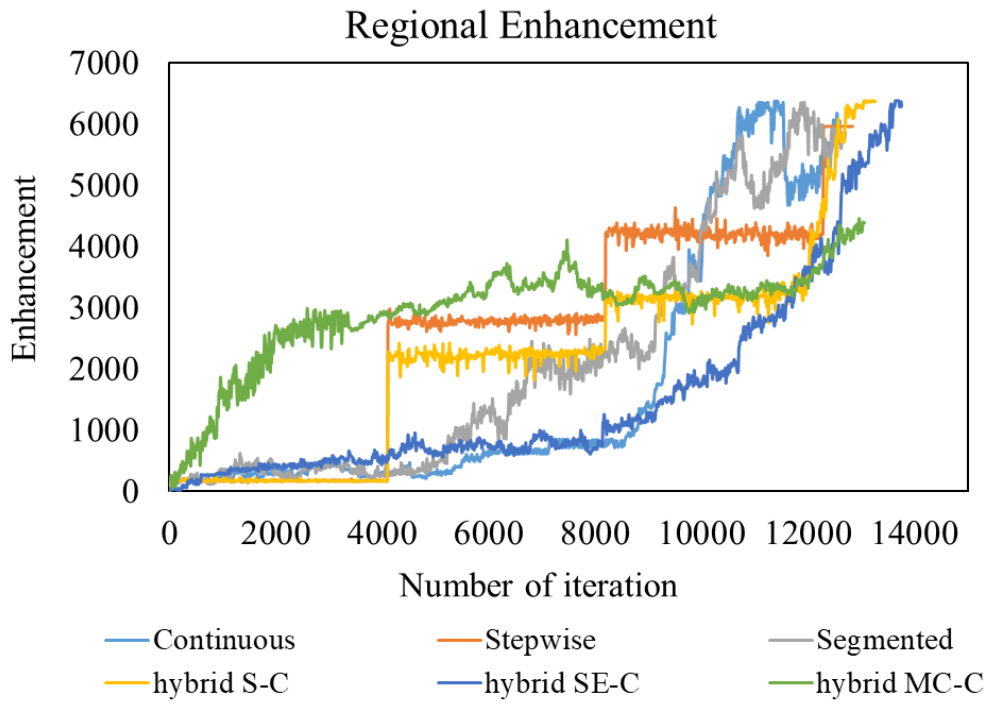

Figure 4.21 Regional enhancement of six algorithms, the performance rank is SC, SEC, C, S, SE, and MCC respectively.

4.1.2.2 Total Enhancement

Total enhancement is increasing proportional with the regional enhancement. Its increasing is more stable than the regional enhancement. The end value of all algorithms are differ from the regional. Total enhancement is calculated as follow;

$$\mu = \frac{I_0}{I_n} \tag{4.3}$$

Where μ is the total enhancement, I_0 is the intensity after optimization and I_n is the before intensity at the target point.

At the end of optimization hybrid step – con algorithm has the highest intensity, its value is just 0.4% higher than the continuous algorithm that is the second highest intensity, see Table 1. The other algorithms are very close final intensity each other except hybrid Monte Carlo-Con. Its final intensity below the 10% than other

algorithms average intensity, see Figure 4.22. However, it is observed that the focusing formation with MCC algorihm is faster than others algoritmhs in the first 4000 iteration. That is parallel with the regional enhancement results Figure 4.22.

Table 6 Summary of the total enhancement of six algorithms

Algorithm Type	**Total Enhancement**	**Total Time (s)**	**Picture**
Hybrid S-C	5.82	2302	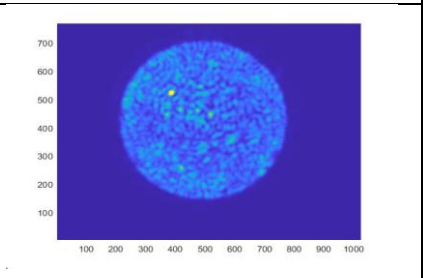
Continuous	5.80	2273	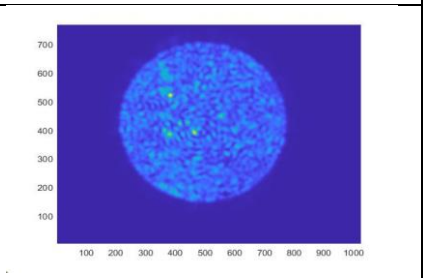
Stepwise	5.61	2335	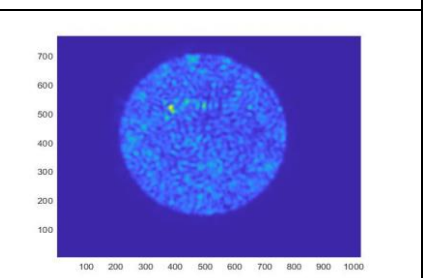
Segmented	5.47	2397	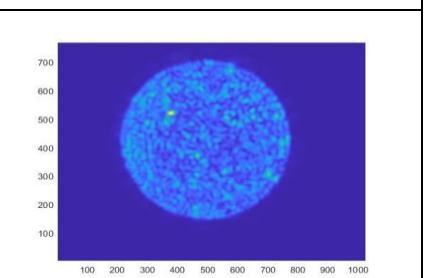

Table 6 (continued)

Algorithm Type	**Total Enhancement**	**Total Time (s)**	**Picture**
Hybrid SE-C	4.97	2336	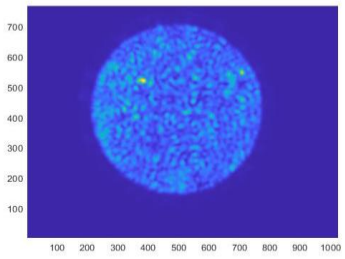
Hybrid MC-C	4.90	2706	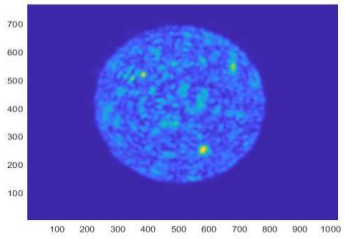

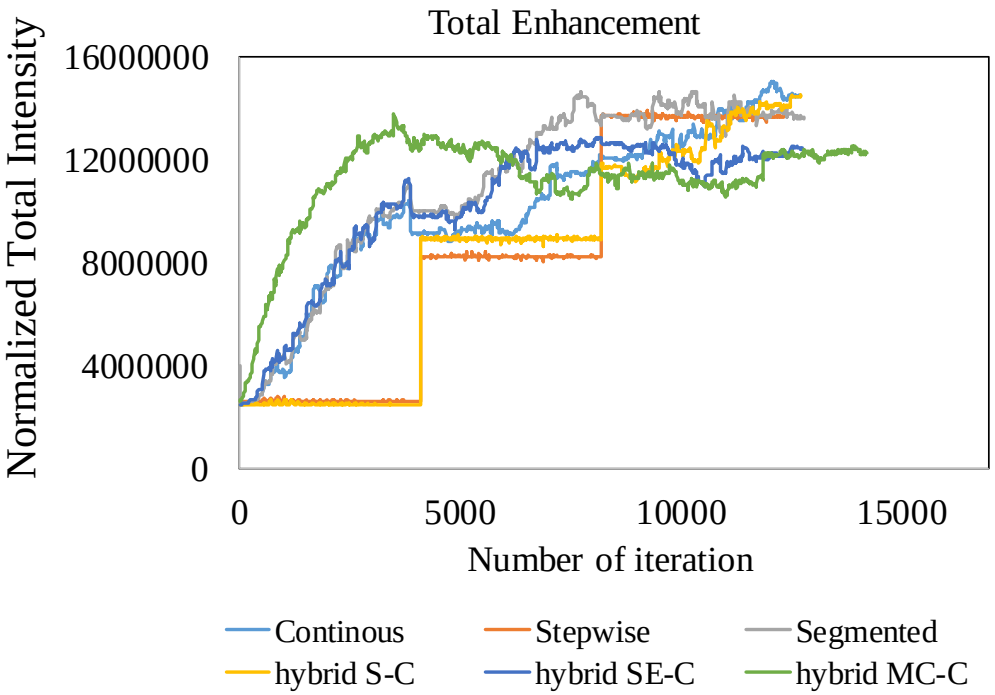

Figure 4.22 Representing total enhancement versus iteration number of six algorithms

CHAPTER 5

CONCLUSION

In this study, we create optimization algorithms for wavefront shaping that focus the light at the target point inside disordered media. One target point with $5x5$ pixels size is selected. These six algorithms are continuous, stepwise, segmented, hybrid stepwise-continuous, hybrid segmented-continuous and hybrid Monte Carlo–continuous. Among the three base algorithms, continuous, stepwise, and segmented, continuous algorithms have reached the best performance for both operation speed and enhancement. The operation speed of continuous algorithm is faster than the stepwise and segmented algorithms 2.7% and 5.1% respectively. The regional enhancement of continuous algorithm is higher than the stepwise 1.1% and %2.9% segmented. The focus threshold value is chooses as 200/255 (0 is black and 255 is white) for 5x5 pixel its value 5000. Then, while the six algorithms running, the continuous algorithm has reached focus faster than the others. The ranking is continuous, segmented, stepwise, hybrid SC, hybrid PC and hybrid MCC respectively. The continuous algorithm 46% faster than the hybrid Monte-Carlo-continuous algorithms. Total focus of light takes a long time for hybrid Monte Carlo-continuous algorithms. However, the starting the focus formation is much earlier than the other five algorithms. The focus can be seen in the 357 seconds for hybrid Monte Carlo –continuous, it takes 1687 seconds for continuous algorithm and 1526 segmented algorithms. The stepwise algorithm is the second fastest method for focus formation with 743 seconds. But, the hybrid Monte Carlo- continuous 208% faster than the stepwise algorithm. If we compare these six algorithms according to the total enhancement; hybrid stepwise-continuous has the higher performance with 5.82 time total enhancement. The ranking is follow; the continuous 5.8, the stepwise 5.61, the segmented 5.47, the hybrid segmented-continuous 4.97, hybrid Monte Carlo-continuous 4.90.

REFERENCES

[1] Méndez, A. (2016). Optics in medicine. *Optics in Our Time*, 299–333. https://doi.org/10.1007/978-3-319-31903-2_13

[2] R., D. H. J. (1998). *Understanding optical communications*. Prentice Hall.

[3] Milne, E. A. (1921). Radiative equilibrium in the outer layers of a star: The temperature distribution and the law of darkening. Monthly Notices of the Royal Astronomical Society, 81(5), 361–375. https://doi.org/10.1093/mnras/81.5.361

[4] Ishimaru, A. (1978). Limitation on image resolution imposed by a random medium. *Applied Optics*, *17*(3), 348. https://doi.org/10.1364/ao.17.000348

[5] Zhu, J. X., Pine, D. J., & Weitz, D. A. (1991). Internal reflection of diffusive light in random media. *Physical Review A*, *44*(6), 3948.

[6] Vellekoop, I. M. (2008). Controlling the Propagation of Light in Disordered Scattering Media, 144 University of Twente.

[7] Sheng, P. (2006). *Introduction to wave scattering, localization and mesoscopic phenomena* (Vol. 88). Springer Science & Business Media.

[8] Hulst, H. C., & van de Hulst, H. C. (1981). *Light scattering by small particles*. Courier Corporation.

[9] Derode, A., Tourin, A., de Rosny, J., Tanter, M., Yon, S., & Fink, M. (2003). Taking advantage of multiple scattering to communicate with time-reversal antennas. Physical Review Letters, 90(1), 014301.

[10] Lerosey, G., De Rosny, J., Tourin, A., & Fink, M. (2007). Focusing beyond the diffraction limit with far-field time reversal. Science, 315(5815), 1120-1122.

[11] Lantz, E., Le Tolguenec, G., & Devaux, F. (2001). Imaging through diffusing media by image parametric amplification. *Waves and Imaging through Complex Media*, 267–273. https://doi.org/10.1007/978-94-010-0975-1_14

[12] Sebbah, P. (Ed.). (2001). Waves and imaging through complex media. Springer Science & Business Media.

[13] C.H. R. Huygens,Traitéde lalumière (vander Aa,Leiden, 1690)

[14] Pappu, R., Recht, B., Taylor, J., & Gershenfeld, N. (2002). Physical one-way functions. Science, 297(5589), 2026-2030.

[15] Goodman, J. W. (2000). Statistical Optics (Wiley Classics Library).

[16] Čižmár, T., & Dholakia, K. (2012). Exploiting multimode waveguides for pure fibre-based imaging. *Nature communications*, *3*(1), 1-9.

[17] Papadopoulos, I. N., Farahi, S., Moser, C., & Psaltis, D. (2013). Increasing the imaging capabilities of multimode fibers by exploiting the properties of highly scattering media. *Optics letters*, *38*(15), 2776-2778.

[18] Binici, H. İ. (2018). *Controlling light inside a multi-mode fiber by wavefront shaping* (Master's thesis, Middle East Technical University).

[19] Davis, J. A., McNamara, D. E., Cottrell, D. M., Campos, J., & Yzuel, M. J. (2001). Encoding complex diffractive optical elements onto a phase-only liquid-crystal spatial light modulator. *Optical Engineering*, *40*(2), 327-329.

[20] Kelly, T. L., & Munch, J. (1998). Phase-aberration correction with dual liquid-crystal spatial light modulators. *Applied optics*, *37*(22), 5184-5189.

[21] Arrizón, V. (2003). Complex modulation with a twisted-nematic liquid-crystal spatial light modulator: double-pixel approach. *Optics letters*, *28*(15), 1359-1361.

[22] Bagnoud, V., & Zuegel, J. D. (2004). Independent phase and amplitude control of a laser beam by use of a single-phase-only spatial light modulator. *Optics letters*, *29*(3), 295-297.

[23] Davis, J. A., McNamara, D. E., Cottrell, D. M., Campos, J., & Yzuel, M. J. (2001). Encoding complex diffractive optical elements onto a phase-only liquid-crystal spatial light modulator. *Optical Engineering*, *40*(2), 327-329.

[24] Hayasaki, Y., Sugimoto, T., Takita, A., & Nishida, N. (2005). Variable holographic femtosecond laser processing by use of a spatial light modulator. *Applied Physics Letters*, *87*(3), 031101. https://doi.org/10.1063/1.1992668

[25] Psaltis, D., Paek, E. G., & Venkatesh, S. S. (1984). Optical image correlation with a binary spatial light modulator. Optical Engineering, 23(6). https://doi.org/10.1117/12.7973366

[26] F. Mok, J. Diep, H.-K. Liu, and D. Psaltis, "Real-time computer-generated hologram by means of liquid-crystal television spatial light modulator," Opt. Lett., vol. 11, pp. 748–750, Nov 1986.

[27] Ross, W. E., Psaltis, D., & Anderson, R. H. (1983). Two-dimensional magneto-optic spatial light modulator for Signal Processing. Optical Engineering, 22(4). https://doi.org/10.1117/12.7973148

[28] I. M. Vellekoop and A. P. Mosk, "Focusing coherent light through opaque strongly scattering media," Opt. Lett., vol. 32, pp. 2309–2311, Aug 2007.

[29] Van Putten, E. G. (2007). *Focussing of light inside turbid media* (Doctoral dissertation, Master's thesis, University of Twente).

[30] Başay, Y. (2018). *Broadband spectral splitting of light using wavefront shaping* (Master's thesis).

[31] Fidanboylu, K. A., & Efendioglu, H. S. (2009, May). Fiber optic sensors and their applications. In *5th International Advanced Technologies Symposium (IATS'09)* (Vol. 6, pp. 2-3).

[32] Grote, N., & Venghaus, H. (Eds.). (2001). *Fibre optic communication devices* (Vol. 4). Springer Science & Business Media.

[33] Birch, P. M., Young, R., Budgett, D., & Chatwin, C. (2000). Two-pixel computer-generated hologram with a zero-twist nematic liquid-crystal spatial light modulator. *Optics letters*, *25*(14), 1013-1015.

[34] Arrizón, V. (2003). Complex modulation with a twisted-nematic liquid-crystal spatial light modulator: double-pixel approach. *Optics letters*, *28*(15), 1359-1361.

[35] Okamoto, K. (2021). *Fundamentals of optical waveguides*. Elsevier.

[36] Dutton, H. J. (1998). *Understanding optical communications* (Vol. 1). Durham, North Carolina, USA: Prentice Hall PTR.

[37] Wadsworth, W. J., Percival, R. M., Bouwmans, G., Knight, J. C., Birks, T. A., Hedley, T. D., & Russell, P. S. J. (2004). Very high numerical aperture fibers. *IEEE Photonics Technology Letters*, *16*(3), 843-845.

[38] Ishimaru, A. (1989). Diffusion Of Light In Turbid Material. *Applied Optics*, *28*(12), 2210-2215.

[39] Barabanenkov, Y. N., & Ozrin, V. D. (1992). Problem of light diffusion in strongly scattering media. *Physical review letters*, *69*(9), 1364.

[40] Narasimhan, S. G., Nayar, S. K., Sun, B., & Koppal, S. J. (2005, October). Structured light in scattering media. In *Tenth IEEE International Conference on Computer Vision (ICCV'05) Volume 1* (Vol. 1, pp. 420-427). IEEE.

[41] Vellekoop, I. M., & Mosk, A. P. (2008). Phase control algorithms for focusing light through turbid media. *Optics communications*, *281*(11), 3071-3080.

[42] Zhou, Y., & Li, X. (2017). Optimization of iterative algorithms for focusing light through scattering media. *IEEE Photonics Journal*, *9*(2), 1-10.

[43] Vellekoop, I. M., & Aegerter, C. M. (2010, February). Focusing light through living tissue. In *Optical Coherence Tomography and Coherence Domain*

Optical Methods in Biomedicine XIV (Vol. 7554, p. 755430). International Society for Optics and Photonics.

[44] Vellekoop, I. M., Lagendijk, A., & Mosk, A. P. (2010). Exploiting disorder for perfect focusing. *Nature photonics*, *4*(5), 320-322.

[45] Marcuse, D. (1982). Light transmission optics. *New York*.

[46] Assous, F., Degond, P., Heintze, E., Raviart, P. A., & Segré, J. (1993). On a finite-element method for solving the three-dimensional Maxwell equations. *Journal of Computational Physics*, *109*(2), 222-237.

[47] Jones, D. S. (2013). *The theory of electromagnetism*. Elsevier.

[48] Vellekoop, I. M., Van Putten, E. G., Lagendijk, A., & Mosk, A. P. (2008). Demixing light paths inside disordered metamaterials. *Optics express*, *16*(1), 67-80.

[49] Garcia, N., & Genack, A. Z. (1989). Crossover to strong intensity correlation for microwave radiation in random media. *Physical review letters*, *63*(16), 1678.

[50] Beenakker, C. W. (1997). Random-matrix theory of quantum transport. Reviews of modern physics, 69(3), 731.

[51] Bagnoud, V., & Zuegel, J. D. (2004). Independent phase and amplitude control of a laser beam by use of a single-phase-only spatial light modulator. *Optics letters*, *29*(3), 295-297.

[52] Holoeye, HOLOEYE Photonics AG Volmerstrasse 1 12489 Berlin, Germany, Pluto-2 Phase Only Spatial Light Modulators, 1.7 ed., 8 2018.

[53] Van Putten, E. G., Vellekoop, I. M., & Mosk, A. P. (2008). Spatial amplitude and phase modulation using commercial twisted nematic LCDs. *Applied optics*, *47*(12), 2076-2081.

[54] S. Rothe, H. Radner, N. Koukourakis, and J. W. Czarske, “Transmission Matrix Measurement of Multimode Optical Fibers by Mode-Selective Excitation Using One Spatial Light Modulator,” Applied Sciences, vol. 9, p. 195, jan 2019

[55] V. Bagnoud and J. D. Zuegel, “Independent phase and amplitude control of a laser beam by use of a single-phase-only spatial light modulator,” Optics Letters, vol. 29, p. 295, feb 2004.

[56] Kahraman, S. S. (2021). *Enhancing the Resolution of Multimode Fiber Based Spectrometers* (Master's thesis, Middle East Technical University).

[57] Gün, B. N. (2020). *Wavefront shaping assisted design and application of effective diffractive optical elements providing spectral splitting and solar concentration: splicons* (Master's thesis, Middle East Technical University).

[58] Di Leonardo, R., & Bianchi, S. (2011). Hologram transmission through multi-mode optical fibers. *Optics express*, *19*(1), 247-254